Numerical methods for load prediction in acoustic fatigue

Nilsson, Johan

2014

Document Version:
Publisher's PDF, also known as Version of record

LUND UNIVERSITY

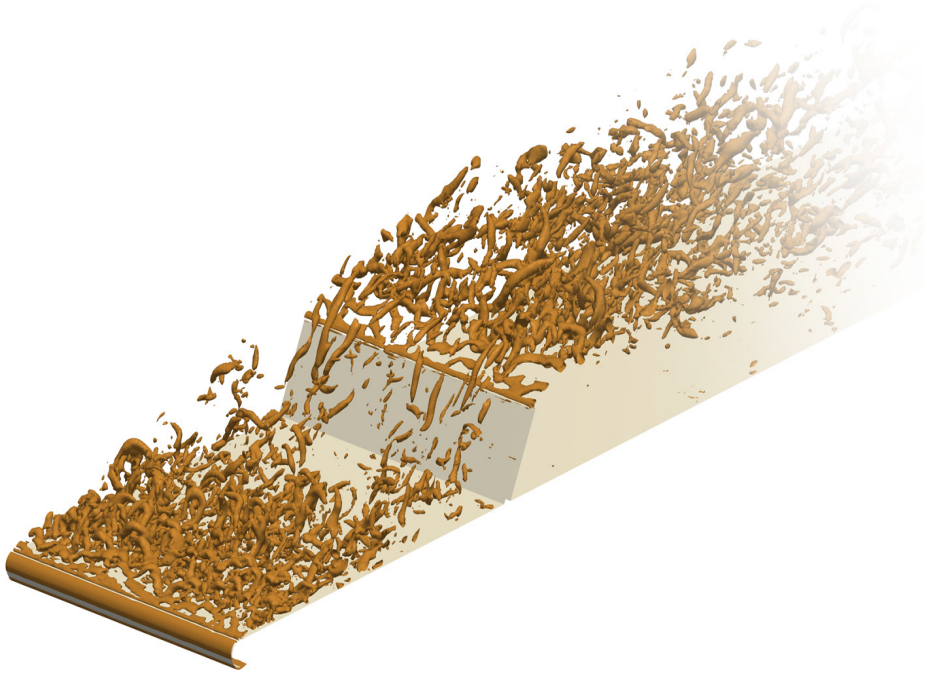

NUMERICAL METHODS FOR LOAD PREDICTION IN ACOUSTIC FATIGUE

JOHAN NILSSON

Structural Mechanics

Licentiate Dissertation

DEPARTMENT OF CONSTRUCTION SCIENCES

DIVISION OF STRUCTURAL MECHANICS

ISRN LUTVDG/TVSM--14/3074--SE (1-99) | ISSN 0281-6679

ISBN 978-91-7623-198-2 (print) | 978-91-7623-199-9 (Pdf)

LICENTIATE DISSERTATION

NUMERICAL METHODS FOR LOAD PREDICTION IN ACOUSTIC FATIGUE

JOHAN NILSSON

Printed by Media-Tryck LU, Lund, Sweden, November 2014 *(Pl)*.

For information, address:

Div. of Structural Mechanics, LTH, Lund University, Box 118, SE-221 00 Lund, Sweden.
Homepage: http://www.byggmek.lth.se

Acknowledgements

The work presented in this dissertation was carried out at the Division of Structural Mechanics, Faculty of Engineering at Lund University, Sweden. The financial support from Sweden's innovations agency VINNOVA and Saab AB under the Fifth National Aviation Engineering Research Programme (NFFP5) is gratefully acknowledged. The simulations were performed on resources provided by the Swedish National Infrastructure for Computing (SNIC) at Lunarc and HPC2N.

This kind of work is not something I could have done without the help of others. First of all I would like to thank my supervisors Dr. Per-Erik Austrell at the Division of Structural Mechanics and Dr. Robert-Zoltán Szász at the Division of Fluid Mechanics for your continuous support, encouragement and guidance. I would also like to thank Prof. Ephraim J. Gutmark at the University of Cincinnati and M.Sc. Karl-Johan Molin at Saab AB for your ideas and resources in our collaboration. I am also grateful for the contributions from Dr. Delphine Bard at the Division of Engineering Acoustics on one of the papers. Furthermore, I would like to thank the staff of Lunarc for your immediate assistance whenever I run into problems on your clusters. The entire staff of the Department of Construction Sciences deserves an acknowledgement for providing assistance in this work as well as providing a friendly working environment.

I would like to take opportunity to thank my parents and my brother for your endless love and support. Finally, I would to like to thank Emma for being understanding, supportive and patient with me during the course of this work.

Lund, November 2014
Johan Nilsson

Abstract

Acoustic fatigue can occur in structural elements of an aircraft exposed to very high sound pressures. To deal with acoustic fatigue, mainly empirical methods have been applied and often late in the design phase. Current design guidelines have several limitations. First, they do not say anything about the load intensities. The load levels can be determined either experimentally or numerically. Experimental testing tends to be expensive and time consuming. It is also desired to deal with acoustic fatigue early in the design phase. Therefore, it is desired to turn to numerical methods to determine the load levels. Second, the design guidelines assume that the spatial distribution of the load is uniform. In other words, the load is assumed to be perfectly in phase over the entire structural element. This assumption limits the accuracy of the response prediction and by extension the fatigue prediction. In order to take the spatial distribution into account it must first be determined.

In this dissertation, load prediction in the context of acoustic fatigue by numerical methods using Computational Fluid Dynamics (CFD) is investigated. From the CFD simulations, both the load intensities and the spatial distributions are extracted. CFD simulations are performed on two model problems where the simulation results are compared to existing measurements on the simulated setup.

In paper A, a ramped backward-facing step is used as a model problem for acoustic fatigue. The flow over the step induces a load on an aluminium sheet fitted downstream of the step. With the exception of the cut-off, or shedding, frequency being overpredicted, the spectral qualities of the load and the load intensities are well captured. The extracted load is used as force input to a Finite Element (FE) simulation of the response of the exposed aluminium sheet. The response prediction is found to be good when compared to design guidelines and other studies where the spatial distribution of the load is considered.

The model problem studied in paper B is flow over an inclined fence at transonic Mach number and realistic Reynolds number for aircraft operation. Load intensities downstream of the fence are well captured. The spatial characteristics in the form of cross-correlations appear to be on the level required for a good response prediction of an aircraft skin surface panel placed downstream of the fence. A sensitivity study of three different geometrical configurations of the solution domain was performed as it was found that the flow is sensitive to what happens upstream of the fence. It is found that the spectral characteristics of the load downstream of the fence is affected by this geometrical sensitivity. Several aspects of the surface load as well as the flow in general are investigated and compared to existing measurements.

Contents

Part I

Introduction and overview of the work

1 Introduction

Acoustic fatigue, also known as sonic fatigue, is a problem for the aircraft industry. Structural elements, such as skin surface panels, on aircraft may be exposed to high intensity sound levels. These high sound levels may cause the structural element to vibrate, simply because sound is pressure fluctuations. This means that the high sound intensities act as fluctuating force loading on the structural element. The vibration may lead to cracks in the structural element and already existing cracks may grow. If this vibration is allowed to go on unchecked it may eventually lead to failure. The vibrational frequencies involved tend to be in the order of hundreds of Hz. Acoustic fatigue can therefore develop quickly as it does not take a long time before a large number of cycles have passed.

There are several possible sources for this high intensity load. The perhaps most obvious source is noise form the jet engine or the propeller. But there is also the case where geometrical features cause strong loads. These may be control surfaces, flaps and cavities. All these geometrical features include separated flow and periodic vortex shedding as key features.

Acoustic fatigue is a problem in several ways. Obviously, aircraft suffering from failure in flight can have drastic consequences. Keeping cracks under control is therefore important. During maintenance the aircraft can be tested for cracks, but not all parts of the aircraft can easily be tested. Frequent maintenance requirements are undesired for economic reasons.

Traditionally, acoustic fatigue has been dealt with using empirical methods. Design guidelines have been developed and are applied. An example of this is the ESDU design guidelines on acoustic fatigue [1]. The current design guidelines have three main limitations:

1. The load levels at the eigenfrequencies of the panel structure must be known.
2. The load is assumed to be fully in phase over the exposed structure, or in other words, the load is assumed to have a uniform spatial distribution.
3. The design guidelines are limited to a simple surface panel with linear response.

The first limitation can arguably be said to be outside the scope of the design guideline and not being a limitation to the guidelines per se. However, the load levels are often determined experimentally. Finding the load levels experimentally from the use of wind-tunnels or flight testing is expensive. It is also desired to handle acoustic fatigue early in the design phase before any flight testing can be done. It is much cheaper to deal with an issue early on compared to when the aircraft has gone to flight testing. The second limitation reduces the accuracy of the response prediction of the structure which in turn reduces the accuracy of the fatigue prediction. The response prediction has been shown to improve significantly if a more realistic load distribution is applied [2, 3]. The third limitation restricts the guidelines to certain structures. For example, composite panels can have large non-linear response which is not covered by the design guidelines.

For the reasons mentioned above, it is desired to use numerical simulations to predict acoustic fatigue. When it comes to determining the dynamical properties of the aircraft structures, the

Finite Element Method (FEM) has been in heavy use for some time now. This avoids the third limitation with design guidelines given above. However, the determination of the load levels and their spatial and temporal characteristics using numerical methods appears to have been less dealt with. This is the domain of Computational Fluid Dynamics (CFD). Most, if not all, of the typical load sources have been studied with CFD. There are many CFD studies on engine noise, cavities etc. Usually, the concern has been on what noise they make or aspects unrelated to acoustic fatigue. The previous of the two is an important application of CFD within the subject of acoustic fatigue. In other words, while having the ability to make accurate fatigue predictions are desirable, removing the source is much better. It can also be used to address limitation number one in the list above. However, attempts to study the intensities *and* the spatial distribution of the pressure fluctuations on the exposed surfaces directly as a tool for making fatigue predicitions is often not attempted. For the important cases of separated flow, there are few numerical studies on the surface pressure fluctuations. Those that exist are performed on Reynolds numbers far below realistic ones for aircraft operations. Also, they do not make the step to do a response prediction of the exposed surface.

The general aim of this dissertation is to improve the load prediction for acoustic fatigue by attempting to use numerical methods in the form of CFD. This can then be applied to an FE model of the exposed structure. It is desired to capture both the load levels and the spatial distribution of the load as both are important parameters that have good potential to improve the response predictions. Knowledge of what is required of the numerical method to produce an accurate load prediction is naturally sought. In paper A, the simulated load is applied to an FE simulation of the response of a simple structure. This is done to estimate how effective a load obtained from CFD can be in the response prediction. However, the focus in this dissertation is on the load prediction rather than the response prediction. A secondary objective is also to increase the understanding of the flow mechanisms that cause the load.

The scope of the dissertation is limited to the loads caused by separated flows. This excludes all loads that appear in the far field. Open cavities are also an example of separated flows wich have the additional phenomenon of Rossiter [4] tones. Neither open cavities nor Rossiter tones are considered in this dissertation.

It should also be mentioned, that while the aim of this dissertation is on acoustic fatigue, the work here should be of interest for efforts to reduce the noise inside the cabin as well. The sound pressure levels discussed are high and the vibration of the outer skin surface panels are clearly a transmission path. Although cabin noise reduction is not directly inside the scope of this dissertation, it should be noted that this work may be beneficial in other contexts as well.

This dissertation is organised in two parts. The second part consists two research papers that have been produced in this project. These papers are preceded by an extended introduction and overview of the work. It also contains a more thorough treatment of topics that are treated in less detail in the papers. Chapter 2 is a literature review on acoustic fatigue. In Chapter 3, the motion of fluids is discussed. This includes a phenomenological discussion of turbulent flow, the numerical treatment as well as an introduction to flow types dealt with in this dissertation. The numerical methods used to predict the structural response in paper A is covered in Chapter 4. Chapter 5 contains a summary of the appended papers. Finally, some concluding remarks and suggestions for future work are given in Chapter 6.

2 Acoustic fatigue

2.1 Introduction

In the early fifties, acoustic fatigue (also known as sonic fatigue) related incidents increased on new jet engined aircraft. This led to a range of experimental studies at several aircraft companies. Since the failures were frequently located near jet engine exhausts, actual aircraft jet engines were often used to provide realistic acoustic excitation on single panel studies, as well as large parts of aircraft strucures. This eventually lead to the development of analytical methods and design guidelines [5,6]. These methods are described in section 2.2. Even though the power of the engines kept increasing throughout the sixties and seventies, the sound pressure levels were not. The reason for this is the development of high-bypass turbofan engines in order to reduce engine noise near airports. The lack of increase in pressure levels together with the now established design guidelines reduced interest in research and development on acoustic fatigue. However, the introduction of composites in aircraft skin panels in the mid eighties and nineties spured new interest in the subject. The composite panels can feature large displacements taking the response into the non-linear region, thus creating new challenges [5, 6]. The work with composite panels is covered in section 2.3. Two studies giving important attention to the spatial distribution of the load are covered in section 2.4. Finally, section 2.5 provides some discussion of the literature on acoustic fatigue and how it relates to the work performed in this dissertation.

A common way to test acoustical excitation of a structure, which also appears frequently in the studies mentioned in this chapter, is the usage of a so called Progressive Wave Tube (PWT). A PWT is essentially a very powerful loudspeaker/siren which can deliver very high sound levels, sometimes up in the region of 165 dB. The sound is then directed through a tube passing over the sample. A typical setup is illustrated in Figure 2.1. The sample is placed so that the sound waves pass over the surface of the sample which is placed on one side of the tube.

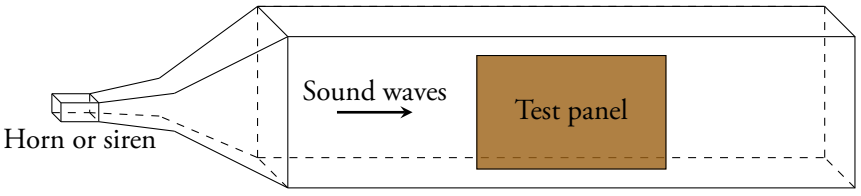

Figure 2.1: Basic layout of a Progressive Wave Tube (PWT) test rig.

2.2 Analytical methods and design guidelines

The first method for response prediction of an acoustically excited metallic structure was developed by Miles [7]. In his study, the skin panel structure was modelled by a single rectangular thin linear-elastic plate. Furthermore, only the response in the fundamental mode was considered, thus turning the model into a single degree-of-freedom system. The load was assumed to be uniform, or in-phase, over the whole plate with a spectral density $G_p(f_n)$ at the frequency of the fundamental mode f_n. From these assumptions, Miles derived the following expression for the mean square stresses for the plate

$$\overline{\sigma^2(t)} = \frac{\pi}{4\zeta} f_n G_p(f_n) \frac{\sigma_0^2}{F_0^2}, \tag{2.1}$$

where σ_0 is the static stress at the point of interest due to a the uniformly distributed force F_0 and ζ is the viscous damping ratio. To estimate the fatigue life of the panel Miles used Miner's cumulative damage hypothesis [8].

Powell [9] took this one step further by considering multiple modes via the normal mode approach. The modes of the plate subjected to the random pressure load were assumed to be uncoupled. This is true if the displacements are small and the structure lightly damped, as is typically the case for metallic aircraft skin structures. The response can then be given as summation of the response in each mode. In addition, he also introduced the concept of "joint acceptance", which is a measure of the effectiveness of the pressure field to excite a particular mode.

Later, Clarkson [10] took Powell's work and suggested a simplification of it in order to develop a relatively simple formulation which could be used in the design of aircraft skin panels. Clarkson showed that if it is assumed that the response is dominated by one mode and the excitation pressures at that mode are in-phase over the whole plate, then the result reduces to Miles equation (2.1), which is still used today as a design tool for structures subjected to random pressure loading. By also assuming that the plate had fully fixed conditions, he propsed a series of steps to be used as a design process.

The IHS ESDU (previously Information Handling Services and Engineering Sciences Data Unit, respectively) provides design guidelines and design data in many different fields such as, areospace engineering, process engineering and structural engineering. Among these, they provide a series on vibration and acoustic fatigue which includes [1] based on the studies presented in this section. Another design guideline based on the same approach is the AGARD method [11]. Furthermore, there is also an extensive text called "Sonic fatigue design guide for military aircraft" [12] on the subject compiled by the Acoustics & Vibration Associates for the US Air Force. It is the result from a review of over 300 references related to acoustic fatigue containing many tables, charts, nomographs, computer programs and worked examples.

Blevins [13] extended Miles' and Clarkson's method to several modes. He also used the concept of joint acceptance which he used when he studied how different spatial distributions of the acoustical load affected the response of the structure. He did not use an exactly known load distribution but looked at a few different approximations, e.g. a sinusoidal load or a load which has the same spatial distribution as the (mass weighted) structural mode. The latter approximation he compared with AGARD's guidelines for a simple rectangular plate and got almost the same result. To determine the mode shapes and the eigenfrequencies of the plate, which is input to the method, he used the FE-software MSC/NASTRAN. He also compared experimental data from a different plate tested in a PWT and found the results from the model higher than the experimental values, but within

the margin of experimental error. While Blevins' work tries to take the load spatial distribution into account, it still requires that some spatial properties of the load is known as well as the load intensity and spectral properties.

2.3 Non-linear behaviour

The methods in section 2.2 were developed with metallic structures in mind and not composites being common in aircraft today. One of the first studies on the response of composites was made by White [14]. He compared measurements of the response of an aluminium plate and a plate made of a carbon fiber composite (CFRP - Carbon Fiber Reinforced Plastic) in a PWT. The CFRP panel exhibited a high degree of non-linearity. For very high sound intensities this was also true for the aluminium panel, but the non-linearities were much lower. As an example, the first eigenfrequency increased 100 % when the excitation increased from 130 dB to 154 dB for the CFRP panel, but for the aluminium panel the corresponding change was only 35 %. The methods described in section 2.2 use the assumption that the panel response is dominated by one or a few modes. The non-linearities at high excitation levels in the CFRP panel caused only 65 % of the mean square strain to be from the resonance peaks, compared to 90 % for the aluminium plate. Therefore, the methods in section 2.2 can not give an accurate prediction of the tested CFRP panel's response. In addition to the frequency shift of the resonance peaks, the peaks also broaden. As these two behaviours are typical for increased damping, it was initally suggested that non-linear damping played an important part in the observed non-linearities [15]. However, later it was demonstrated by Reinhall and Miles that the broadening and phase shifts could be observed without any non-linear damping [16]. They found the dominant non-linearity to be the increased in-plane stiffness due to the large deflections as accounted for in the von Kármán theory. This increased stiffness is proportional to the cube of the displacements.

Using FE simulations is one way to treat the described geometric non-linear behaviour. However, the computational resources needed to do this directly for a full model in the time domain is very large [17]. Therefore, it is desired to use some form of reduced order modelling (ROM) to lessen the computational burden. A comparison of ROM methods to deal with geometrical non-linearities for acoustic fatigue response predicition can be found in [18]. For hypersonic vehicles thermal loads must also be taken into consideration. A good example of this is the case study found in [19]. Thermal loads can create in-plane stresses causing thermal buckling or snap-through. This makes the analysis more complex as fluid-thermal-structure coupling must be considered [20]. A recent review for ROM that also covers thermal loads and has a focus on using commercial FE-software is found in [21].

2.4 Studies on the impact of the spatial distribution

Cunningham et al. [3, 22] performed experimental and numerical studies on how doubly curved rectangular composite plates behave in a PWT. This study is given a more detailed coverage as some of their key findings relates to some of the fundamental ideas of this dissertation. In their study, they applied single degree-of-freedom models (as described in section 2.2), Blevins [13] method (see section 2.2) and an FE-analysis, in order to predict the panel response. The mode that was excited

the most in the experiment was chosen for the single degree of freedom model, which in neither plate was the fundamental mode. The actual mode shape used was produced in an FE-analysis.

As excitation to the single degree-of-freedom model, three different spatial distributions of the sound pressure field were used. Case 1: Uniform distribution over the whole plate (essentially as Miles and Clarkson). Case 2: The distribution matches that of the excited mode (similar to the assumption tested by Blevins). Case 3: The pressure field forms a sound wave which propagates over the plate with the measured propagation velocity. The different pressure field distributions were applied by computing the joint acceptance. In the first case the response is severely underpredicted. This is due to the fact that a pressure field in phase over the whole plate excites mainly the fundamental mode and excites the higher modes very little, including the one chosen for the model, which gives small strains. They concluded that the problem is not that the wrong mode had been selected, but rather that the actual pressure distribution is very different from the applied pressure distribution. The assumption about the uniform pressure distribution is useful when the acoustical wave length is considerably longer than the plate, which apparently was not the case. In case 2, the response is overpredicted. In this case the pressure distribution gives the joint acceptance equal to 1, which means that the distribution excites the structure at that mode with maximum efficiency. A perfectly matching spatial distribution is in practice unlikely, but maybe case 2 can be seen as a worst case scenario. The approximation of the pressure distribution used in case 3 gave the best prediction and is believed to be a good approximation of the actual one.

When Cunningham et al. tried Blevins method [13] they got similar results as the single degree model for the three different load cases. The third method they tried was an FE-analysis with ANSYS. They used a harmonic solution method where the load was once again simulated as a wave propagating across the plate for each frequency. The FEA underpredicted the r.m.s. strains slightly but was most often within 30 % from the measured values. The result can be compared to the design guidelines which seem to be able to predict the strains only to a factor of 2 compared to measurements [5]. This illustrates that there is a great potential for improvements if the spatial distribution of the load is taken into consideration.

From the September 1st, 1990 to February 28th, 1993 a large EU financed project within the Brite-Euram programme called ACOUFAT, "Acoustic fatigue and related damage tolerance of advanced composite and metallic structures" was carried out. The project involved many of the major European aircraft manufacturers, related contractors, universities and research institutes. Reference [23] contains the final report, which is also published as part of a book [24].

Several different type of activities were carried out by the ACOUAFT project. The first activity was material testing of two metal-alloys and three composite materials. Second, five panel structures of different materials (both metallic and composite) were manufactured. These panels were the subject of modal tests, linearity checks, PWT-testing and FE-modelling. They were designed to be representative of an outer skin-panel of an aircraft. They had a thin upper plate on top of a stringers and ribs arrangement with a thicker lower plate at the bottom for structural rigidity. The lower, thick, plate had cut-outs in each bay to avoid cavity effects and low frequency modes of the total box. Figure 2.2 illustrates the basic design.

The third activity of the ACOUFAT project was a wind-tunnel testing campaign. An aluminium skin panel with a basic design similar to the one shown in Figure 2.2 was flush mounted on a table just downstream of a fence in a wind-tunnel as illustrated in Figure 2.3. As the flow is deflected by the fence, it separates and induces a pressure load on the panel. This type of flow is discussed in section 3.2. The load was measured as well as the panel response to the load. The panel structure

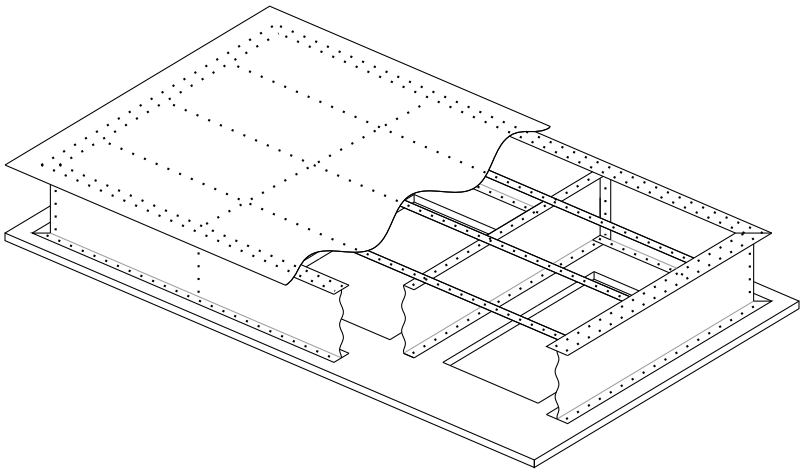

Figure 2.2: Basic panel design.

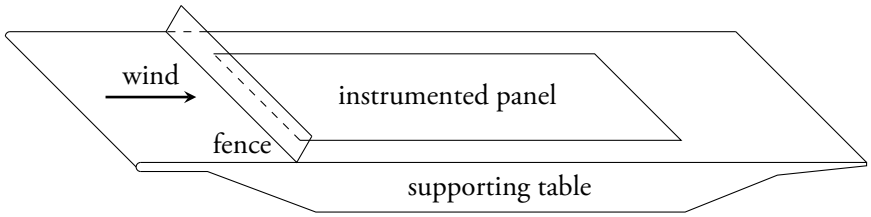

Figure 2.3: Test setup of the wind tunnel table.

used in the wind-tunnel testing was then also tested in two different PWT:s for comparison. The excitation spectrum used in the PWT was formed to match the spectrum measured in the wind-tunnel test. The purpose of performing this comparison was to investigate to what extent PWT testing is representative of more realistic flight conditions. In addition, an attempt to model the load analytically was done by Campos [2, 25]. He developed a semi-emipirical model of the correlation of the wind-tunnel load between different points on the panel. Finally, Campos' model, as well as measured loads from both the wind-tunnel and the PWT measurements, was applied to a FE-model of the panel simulating the panel's response in order to determine the effectiveness of Campos' model. The details of this part of the ACOUFAT project is found in several reports internal to the project [25–29]. In addition, a journal article by Campos et al. includes the semi-empirical model and its application to the FEA of the panel response, as well as the wind-tunnel and PWT-testing comparison [2].

The main findings from the wind-tunnel and PWT-testing comparison related to the spatial correlation of the load and its influence on the panel response. In the PWT measurements, the coherence functions were found to be high, meaning that the acoustic field was nearly fully in phase over the whole panel. Note that this is the assumption used by Miles [7] when deriving equation (2.1), as well as the design guidelines based upon the same idea (see section 2.2). In contrast, the wind-tunnel measurements indicated a much lower coherence or correlation between different points on the panel. A second difference was found in the excitation spectrum in the PWTs. The excitation spectrum was shaped to match the fairly smooth wind-tunnel spectrum measurements. However, the measured pressure load spectrum on the panel in the PWTs were

rather peaky. These peaks are caused by standing waves associated with the inner dimensions of the wave tube.

The measured panel response was found to be different in the PWTs compared to the response measuered in the wind-tunnel. In the wind-tunnel, mainly the anti-symmetrical modes were excited with a symmetry line taken at the centre-line in the streamwise direction. The opposite was found in the PWTs; there the symmetrical modes were the ones that were excited. The FE-simulation of the panel response was performed in the frequency domain with the auto-spectra shaped as the wind-tunnel measurements. In order to investigate the influence of the load coherence on the panel response a parameter study was performed where the coherence, or cross-spectra, was varied between 0 and 1, with the same cross-spectra over the whole panel. For low values of the coherence the response was similar to that in the wind-tunnel measurements; mainly anti-symmetrical modes were excited. On the other hand, a high coherence would excite mainly the symmetrical modes. Also, when applying the measured cross-spectra from the wind-tunnel, a similar response to the wind-tunnel measurements appeared.

The analytical, or semi-emipirical, model of the spatial correlations of the wind-tunnel load by Campos is described in [2] and [25]. The model uses sophisticated concepts of math and statistics. It is based on the idea that the turbulent wake (the shear layer) emits sound that may be decomposed into plane waves. These waves may then reflect against the panel surface and against the wake itself. Since the wake is turbulent, it has an irregular shape. This irregularity means that the distance a sound wave emited from the wake has to travel in order to reach the panel surface differs from different points in time and space. This causes random phase shifts, which are considered in the model as well. The model requires no less than eight parameters to be given. These are:

1. Double reflection coefficient.
2. Excitation frequency (this is a strong tonal frequency found in the wind tunnel load).
3. Longitudinal excitation wavenumber.
4. Transverse excitation wavenmumber.
5. Root mean square phase shift.
6. Longitudinal correlation scale.
7. Transversal correlation scale.
8. Correlation time.

The spatial correlation predicted by the model corresponds well to the wind-tunnel measurements on some microphones pairs, and worse on others. Nevertheless, when the model is used as input to the FEA of the panel reponse, the response is predicted remarkably well.

From the wind-tunnel and PWT comparison, as well as the semi-empirical modelling, some conclusions were made by the ACOUFAT project: PWT testing can not reproduce the wind-tunnel loads by merely correctly shaping the spectral contents of the load. The panel response in the PWT is different from the response in the wind-tunnel; in the PWT symmetrical modes are excited, while in the wind-tunnel anti-symmetrical modes are excited. This is important since it could lead to different modes of failure in the PWT-testing as opposed to actual flight conditions. From the correlation paramater study using FE-simulations, the conclusion was drawn by the project that the key load parameter to which modes of the panel that will be excited is the spatial correlation. As the FE-modelling of the panel response was succesful when the correct load characteristics was used, either from measurements or the semi-empirical model, this is not really a new structural phenomenon, but merely a matter of obtaining the right loads.

2.5 Discussion

As the preceding sections of this chapter indicate: a good load specification is essential for a good response prediction of the skin panels. In the early methods covered in section 2.2, that are still used in up to date design guidelines [1], the main formula used (which is similar to equation (2.1)), relies on the information of the load level ($G_p(f_n)$) at a given frequency (f_n). This must by some means be determined. The great improvements to the response prediction that the consideration of the spatial distribution of the load can give is well illustrated by both the studies by Cunningham et al. [3, 22] and the ACOUFAT project (section 2.4). Interestingly, the ACOUFAT study finds that when modelling PWT tests numerically, the cross-correlation of the load should be close to one, meaning the load should be considered to be nearly in phase over the whole panel. On the other hand, Cunningham et al. finds that in order to improve the numerical response prediction of a PWT test, one should not consider the load to be in phase, but rather as wave traveling over the panel. There are, however, some differences between the investigations. The ACOUFAT project focused on the difference between PWT testing and the more realistic conditions found in a wind tunnel, rather than seeking to improve the response prediction in a PWT test. Nevertheless, both investigations underline the importance of the spatial distribution of the load.

To use any method described so far in this chapter, the user must know the load levels (and preferably, the spatial distribution of the load as well). The most obvious way is perhaps to make an actual flight test and measure it. While testing for acoustic fatigue in the most realistic conditions should give the best results, it is desired to avoid this for several reasons. First, the flight tests themselves are expensive and time consuming. Instruments must be fitted and a process of proving air-worthiness may need to be performed (as a result of fitting instruments) before the aircraft can even leave the ground. Second, flight testing a complete aircraft is only possible late in the design process. At this stage many design choices may be fixed and changes can be costly. Therefore it is desired to consider acoustic fatigue early in the design process. Wind-tunnel testing is also expensive and time consuming, but clearly an option. Analytical modelling was also investigated by Campos (as described above) [2]. Despite the fact that the FE-simulations predicted the panel response remarkably well when Campos' model was used, it still requires many parameters to be determined by some means. For this reason the approach is considered to have the same issues as the experimental methods.

Rather than using experimental methods to determine the load, it is desired to turn to numerical methods. This is what is attempted in this dissertation, via the use of Computational Fluid Dynamics (CFD). Using CFD would make it possible to make load predictions early in the design process and without resorting to the expensive physical testing. From a good CFD simulation load intensity, as well as spectral characteristics and spatial distribution, can be extracted. The purpose of the CFD simulation would be to simulate the aerodynamical effect that creates the load directly. If the exposed structure is located in the near-field of the aerodynamical effect, the load can be extracted directly from the CFD simulation. One example of this is the case of separated flow.

In the near field of a transonic flow case, the term acoustic fatigue becomes a bit misleading due to the fact that it becomes difficult to distinguish between acoustic loads and hydrodynamic loads. Thus, it is more suitable to just call these a pressure load. For cases where the exposed structure is located in the far field, it may be needed to simulate the acoustic load source without the domain extending all the way to the exposed surface in order to reduce the computational cost. The load would then have to be transfered to the structure via some kind of wave-propagation method, for

example the use of acoustic analogies. This touches the domain of Computational Aero Acoustics (CAA). A good book on CAA, including examples relevant for acoustic fatigue is [30]. In this dissertation, only problems where the exposed structure is placed in the near-field are studied. CFD is discussed in more detail in section 3.3.

A benefit of using a load generated by CFD is that it can be used as input to a FE-simulation of the panel response. Using the FEM to simulate the panel structure enables good response predictions of more complex structures. In contrast, equation (2.1) assumes a single rectangular metallic plate. Also the ESDU [1] design guidelines make similar assumptions. Composite panels can benefit from FE-simulations as their modeshapes and eigenfrequencies may not be as simple to predict as those of a rectangular plate. Also they exhibit non-linear response more frequently, which can be modeled using FEA, see section 2.3.

3 Fluid motion

3.1 Turbulent flow

3.1.1 Turbulent and laminar flow

Most fluid flows encountered in industrial applications are turbulent. The flows studied in this dissertation are no exceptions; in fact, the turbulent nature of the flows in this dissertation is essential. Turbulent flow is characterised by being chaotic, irregular and random. In contrast, laminar flow is smooth and orderly. Another characteristic for turbulent flow is high Reynolds number, Re, which was introduced by Reynolds (and later named after him) in his classic experiment from 1883 [31]. The Reynolds number is defined as

$$\mathrm{Re} = \frac{UL}{\nu} = \frac{\text{Inertial forces}}{\text{Viscous forces}},$$

where U is a characteristic velocity of the flow, L is a characteristic length of the flow and ν is the kinematic viscosity of the fluid. It is a dimensionless number characterising the ratio between the inertial and the viscous forces of the flow. In Reynolds' experiment, he had water flowing through a straight glass pipe using streaks of dye for visualisation. He found that when the flow was below a certain critical Re, the streak of dye would remain straight and undisturbed; the flow was laminar. Above the critical Re, the dye streak would be disturbed, irregular and chaotic; the flow became turbulent. This is illustrated in Figure 3.1. While the critical Re is different for every specific flow, turbulent flow tends to be characterised by high Re and laminar flow by low Re. In other words, when the inertial forces become too large compared to the viscous forces, the flow becomes turbulent. There are some more features of turbulent flow worth mentioning. First, mixing is much faster in turbulent flow than in laminar flow. Both mass, momentum and heat transfer is enhanced by turbulent flow. Second, turbulent flows contain a large range of length and time scales (which will be further discussed in section 3.1.2). Finally, note that turbulence is a property of the flow, not the fluid.

3.1.2 Scales of turbulence and energy cascade

As already mentioned, one of the features of turbulent flow is the large range of length and time scales. This feature is what makes numerical simulation of turbulent flow so difficult and demanding. Therefore some understanding of these disparate length-scales and how they interact according to the energy cascade theory are necessary. Richardson [32], who introduced the important concept of the energy cascade, summarised the process both concisely and poetically with:

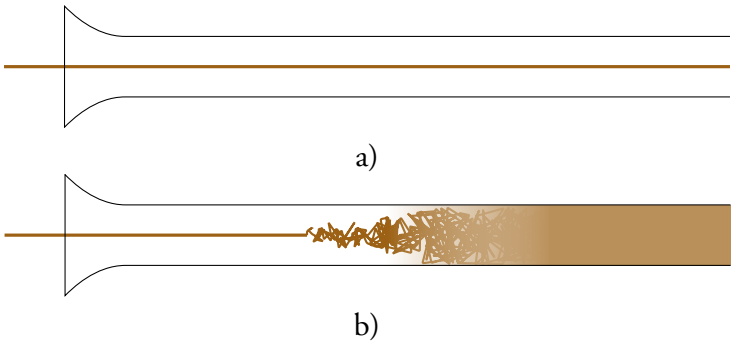

Figure 3.1: Reynolds experiment: a) laminar flow and b) turbulent flow. Sketched after [31].

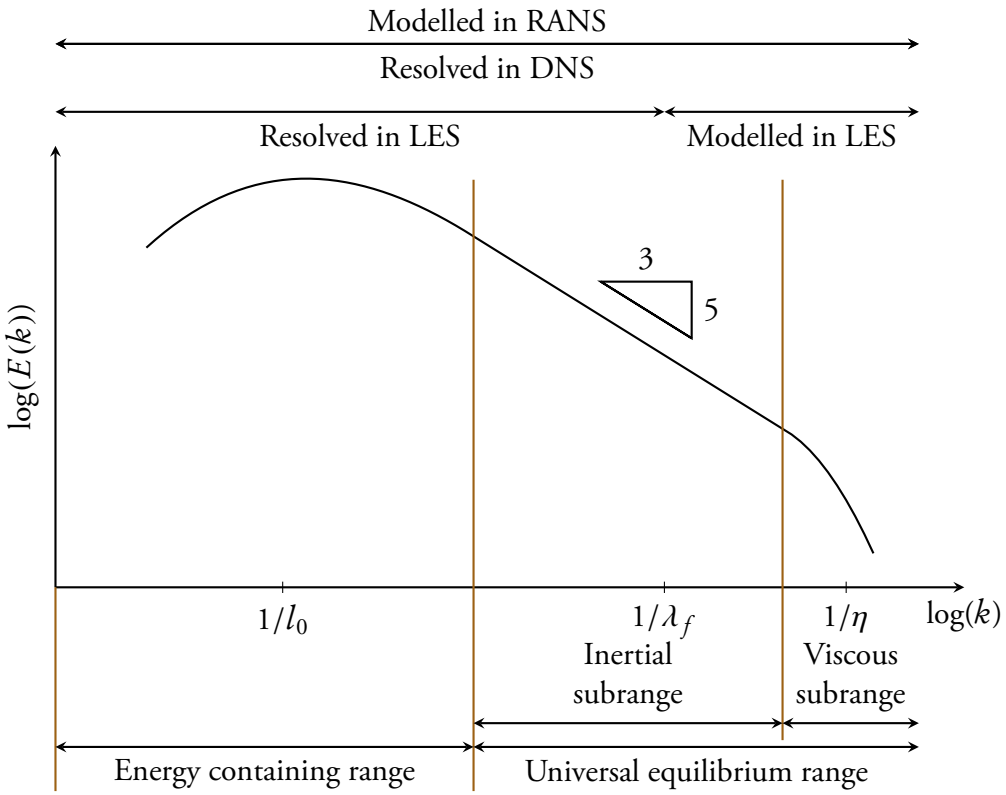

Figure 3.2: Turbulent kinetic energy spectrum $E(k)$ as function of wave number k.

Big whirls have little whirls
that feed on their velocity,
and little whirls have lesser whirls
and so on to viscosity –
(in the molecular sense).

Turbulence is traditionally considered to be composed of eddies of different sizes. An eddy is a localised turbulent flow structure or motion. They also have a characteristic velocity and time scale dependent on the length scale. Figure 3.2 shows a schematical spectrum for the turbulent kinetic energy as a function of the wave number for a typical homogeneous turbulent flow. The wave number can be interpreted as the inverse of the eddy length scale. The spectrum shown in

Figure 3.2 is divided into three zones, each characterised by a lengthscale. These are from the lowest wavenumber to the highest:

1. The energy containing range and the integral length scale l_0.
2. The inertial subrange and the Taylor microscale λ_f.
3. The viscous subrange and the Kolmogorov length scale η.

The integral length scale l_0 is representative for the largest eddies and is of the same order as the characteristic length of the flow, for example the pipe diameter, wing chord length (in this dissertation the step or fence height h is used). It contains more energy than the smaller eddies and therefore characterises the energy containing range. The eddies in this region tend to be highly anisotropic. In contrast, the smaller scales can be approximated to be isotropic according to Kolmogorov's hypothesis of local isotropy [33][1] (somewhat reformulated as according to Pope [35]):

> **Kolmogorov's hypothesis of local isotropy.** At sufficiently high Re, the small scale turbulent motions ($l \ll l_0$) are statistically isotropic.

According to the theory of the energy cascade, large eddies break up into smaller eddies. The small eddies then further break up into even smaller eddies and the process continues until the turbulent kinetic energy of the eddies are dissipated into heat by viscosity. It should be noted that this is true for the process as a whole or on statistical level. Smaller eddies can combine to larger ones and this is known as backscatter. The length scales where the dissipation dominates is called the viscous subrange which is characterised by the Kolmogorov length scale η. This theory is also based on Kolmogorov's hypotheses [33]:

> **Kolmogorov's first similarity hypothesis.** At sufficiently high Re, the statistics of the small scale motions have a universal form that is uniquely determined by the viscosity ν and the dissipation rate of turbulent kinetic energy ε.

The size range defined by the hypothesis is referred to as the universal equilibrium range which is divided into the inertial subrange and the viscous subrange. In the viscous subrange the flow is dominated by viscous forces as discussed above. In contrast, in the inertial subrange the viscous effect are small and the motions are dominated by inertial effects. The inertial subrange is characterised by the Taylor microscale λ_f and is defined by:

> **Kolmogorov's second similarity hypothesis.** At sufficiently high Re, there is a range of scales l such that $\eta \ll l \ll l_0$ that have a universal form that is uniquely determined by the dissipation rate of turbulent kinetic energy ε and independent of the viscosity ν.

The idea that smaller turbulent scales have a statistically universal and isotropic behaviour as described above, makes it sensible to try to approximate their behaviour by some model rather than spending the resources necessary to resolve all lengthscales completely. This is the basic idea of Large Eddy Simulation (LES) which will be discussed in section 3.3.2.

[1] An English translation of the original paper in Russian is available as [34].

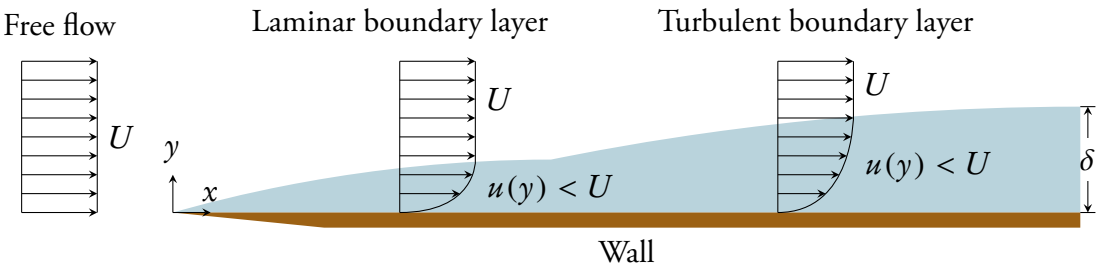

Figure 3.3: Boundary layer over a flat plate. U is the outer velocity and $u(y)$ is velocity in the boundary layer.

3.2 Separating/reattaching flow

3.2.1 Turbulent boundary layer

At the wall, the velocity of the fluid is exactly zero (or in the case of moving walls, the velocity is the same as that of the wall). This is called no-slip. As a consequence of this, there will be a velocity gradient next to the wall and a boundary layer will form. In Figure 3.3, flow over a flat plate is illustrated. Upstream of the plate the velocity profile is uniform. As the flow comes in contact with the plate, the plate will slow the flow down and a laminar boundary layer will form which is coloured in light blue. If the Reynolds number is sufficiently high, the flow will become turbulent which is illustrated further downstream. Important to note is that the boundary layer continues to grow with increasing x. The boundary thickness δ is defined as the distance from the wall where the velocity is 99 % of the external velocity U. An approximate expression for δ in turbulent flows is [36]

$$\delta \approx \frac{0.16x}{\mathrm{Re}_x^{1/7}},$$

where $\mathrm{Re}_x = \rho U x/\mu$ is the local Reynolds number of the flow along the plate surface and x is given in Figure 3.3. The fact that the turbulent boundary layer grows as the flow moves downstream has an important implication for the backward-facing step flow in paper A. This required the implementation of a boundary condition in OpenFOAM which will be described in section 3.3.6.

3.2.2 Backward-facing step flow

Flow over a backward-facing step is a classical test case for CFD. Despite having a very simple geometry it creates a complex flow. There are numerous experimental and numerical studies on this geometry in the literature. The main features of backward-facing step flow are illustrated in Figure 3.4. Upstream of the step, the flow is attached to the wall with a turbulent boundary layer. As the flow reaches the step edge, the flow separates forming a shear layer. The flow reattaches at some distance downstream. The mean reattachment length x_r is generally within the range $5h < x_r < 8h$ [37] where the h is the step height as given in Figure 3.4. The point of reattachment is not fixed but moves in time. Just upstream of x_r is the intensity in the surface pressure fluctuations the highest. The step continues to influence the flow further downstream of the reattachment zone.

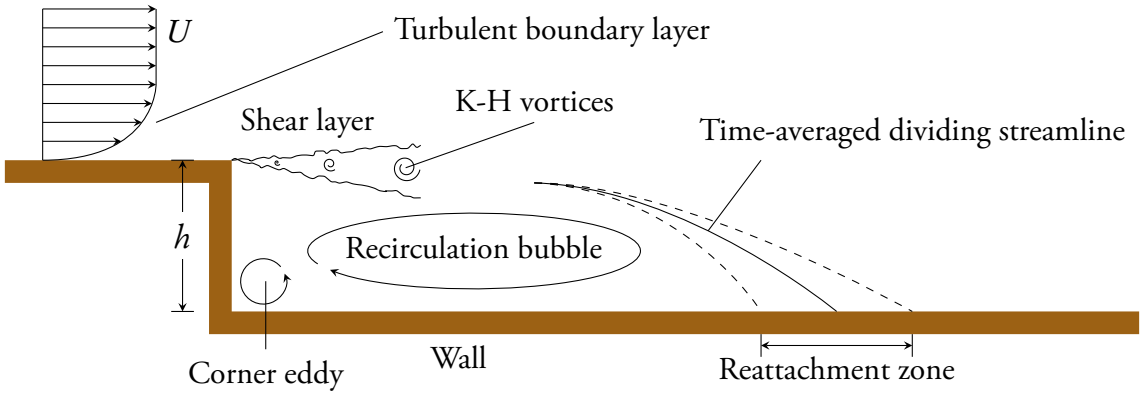

Figure 3.4: Schematic flow over a backward-facing step.

In terms of surface pressure fluctuations, the distance until regular turbulent boundary layer levels are recovered can be as large as 175 h [38]. Underneath the shear layer there is a clockwise rotating recirculation bubble (assuming flow from left to right as in Figure 3.4). In addition, there is a smaller counter-clockwise rotating corner eddy at the bottom corner of the step.

There are two instabilities commonly observed in backward-facing step flow. The first instability causes long spanwise structures known as Kelvin-Helmholtz (K-H) vortices to be shed form the step edge. These structures reduce to the shedding mode via one or more vortex merging processes as described by Hasan [39]. The shedding frequency is typically found to be in the range of $0.6 < \mathrm{St}_{x_r} < 0.8$ where $\mathrm{St}_{x_r} = f x_r / U$, f is the frequency and U is the freestream velocity. There is an important interaction between the turbulent boundary layer and the K-H vortices. The incoming turbulence helps the break up process of the K-H vortices. This reduces the surface pressure fluctuations downstream of the step. This is further discussed in relation to the inlet BC used in paper A in section 3.3.6. The second instability is the absolute instability of the recirculation bubble. The instability is associated with the flapping motion of the shear layer. The flapping frequency is typically found in the range of $0.12 < \mathrm{St}_{x_r} < 0.18$. It should be noted that there are different opinions about the physical explanation of the phenomenon observed as the flapping frequency. A compilation of shedding and flapping frequencies as well as mean reattachment length of many studies on backward-facing step flow is found in Dandois et al. [37].

The backward-facing step flow is used as model problem in paper A with a small variation. The wall that is upstream to step edge in Figure 3.4 is parallel to the downstream wall. This is not the case in paper A. There, the upstream wall is a ramp with an inclination of 6.3°. The general flow characteristics described in this section remain the same.

3.2.3 Fence flow

Another type of separating flow is fence flow. This type of flow is less studied than the backward-facing step flow, particularly numerically. The typical case of fence flow uses the kind of geometry as illustrated in Figure 3.5c. It consists of a splitter plate with a fence upstream. The general characteristics for fence flow are similar to that of backward-facing step flow, but with some differences. The mean reattachment length tends to be longer and with a larger variation. Values in the range $10h < x_r < 34h$ are found in the literature.

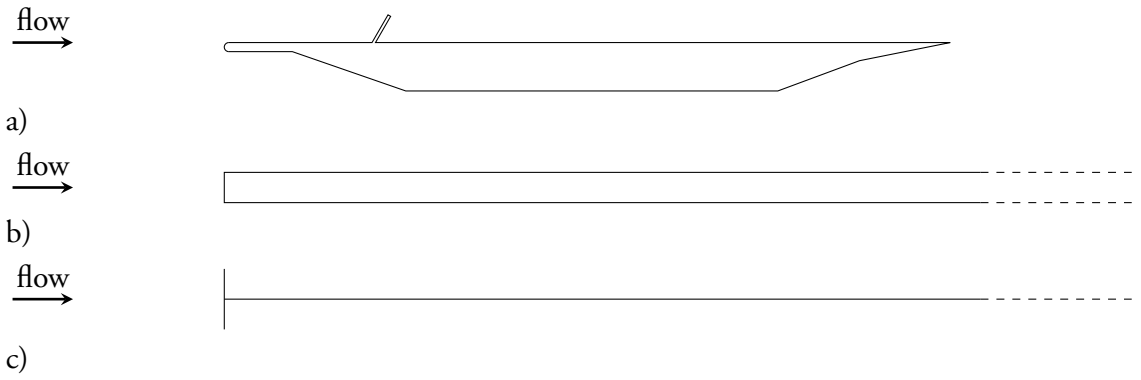

Figure 3.5: The geometry of different fence flow studies. a) is used in ACOUFAT [24], b) is used in Cherry et al. [40] and c) is used in Hudy et al. [41]

The intensity in the maximum surface pressure fluctuations is more severe in fence flow compared to backward-facing step flow. For the backward facing-step the r.m.s. value of the surface pressure fluctuations p'_{rms} is typically around $p'_{\text{rms}}/0.5\rho U^2 = 0.035$, where ρ is the fluid density and U is the freestream velocity. This can be compared to the experimental study by Hudy et al. [41] which found $p'_{\text{rms}}/0.5\rho U^2 = 0.16$ and the experimental study by Cherry et al. [40] which found $p'_{\text{rms}}/0.5\rho U^2 = 0.125$. However, the study by Cherry et al. [40] used the blunt face splitter plate geometry illustrated in Figure 3.5b. An inclined fence as illustrated in Figure 3.5a is used as a model problem in paper B. This geometry was also used in the ACOUFAT project [24]. The simulations in paper B and the measurements in the ACOUFAT project [24] found the maximum $p'_{\text{rms}}/0.5\rho U^2 = 0.06$ and $p'_{\text{rms}}/0.5\rho U^2 = 0.05$, respectively. This is far below the values found by Hudy et al. [41] and Cherry et al. [40]. It is suggested in paper B that this is due to the interaction, or lack thereof, between the incoming turbulence and the shed K-H vortices. For fence flow geometries in Figures 3.5b and 3.5c, there is no incoming turbulent boundary layer and therefore the strong K-H vortices will have a slower break-up rate. The leading edge in Figures 3.5a does cause some turbulence which may interact with the shed K-H vortices. The pressure fluctuation intensity in paper B is still higher compared to backward-facing step flow. The reason for this is likely due to the difference in geometry and the thinner boundary layer in the fence flow case.

3.3 Numerical methods

The numerical treatment of fluid flow is discussed in this section. In this dissertation, the software package OpenFOAM [42] is used. It is open source, released for free under the GNU General Public License and is maintained by the OpenFOAM foundation which is sponsored by the ESI group. OpenFOAM uses the finite volume method and has become very popular in recent years. Part of its popularity probably stems from the fact that there are no license costs and that it can be used for parallel computing via OpenMPI without additional per cpu license costs. It is written in C++ making heavy use of the object oriented programming, templates and operator overloading. This is used to create a syntax for tensor operations and partial differential equations that looks similar to the equations written in mathematical notation, thus facilitating the development of new solvers. It also lends itself to implementation of other extensions such as new turbulence models or boundary

conditions. However, the code is poorly documented and the class relationships can be very complex making the learning curve steep. The lack of extensive documentation does not only apply to the source code itself, but also for general usage. OpenFOAM does come with some mesh generation and manipulation tools such as a block mesher and a tool that makes an unstructured mesh around a geometry file. However, it does not include any pre-processing Graphical User Interface (GUI) and instead comes with a large set of mesh converters from other software. The third party post-processor ParaView is used as OpenFOAM does not contain a post-processor of its own. OpenFOAM runs on Linux only, but there are third party ports for other operating systems.

There are several different topics that need to be addressed to have a full working numerical method. The governing equations of viscous flow will be stated and some of their properties will be discussed in section 3.3.1. The present limits of computational power dictate the use of turbulence modelling which will be discussed in section 3.3.2. The near wall regions are especially demanding, requiring wall treatment that is discussed in section 3.3.3. The discretisation methods used in both space and time are discussed in section 3.3.4. A solver algorithm is needed to produce a solution and this is covered in section 3.3.5. Finally, an inlet boundary condition implemented in OpenFOAM that is used in paper A is described in section 3.3.6.

3.3.1 Governing equations

Viscous flow is governed by the Navier-Stokes equations which is a system of non-linear partial differential equations. They consist of the continuity equation (3.1), momentum equations (3.2) and the energy equation (3.3), here given in conservative form:

$$\frac{\partial \rho}{\partial t} + \nabla \cdot (\rho \mathbf{u}) = 0, \tag{3.1}$$

$$\frac{\partial (\rho \mathbf{u})}{\partial t} + \nabla \cdot (\rho \mathbf{u}\mathbf{u}) = -\nabla p + \nabla \cdot \boldsymbol{\tau} + \rho \mathbf{b}, \tag{3.2}$$

$$\frac{\partial (\rho e_0)}{\partial t} + \nabla \cdot (\rho e_0 \mathbf{u}) + \nabla \cdot (p\mathbf{u}) = \nabla \cdot (k \nabla T) + \nabla \cdot (\boldsymbol{\tau} \boldsymbol{u}), \tag{3.3}$$

where e_0 is the total specific energy, $\boldsymbol{\tau}$ are the viscous stresses (a second order tensor), $\mathbf{b}$ are the body forces, T, ρ, $\mathbf{u}$ and p are the fluid temperature, density, velocity and pressure, respectively. The system needs to be closed with equations of state. In this dissertation with the fluid being air, a calorically perfect gas is assumed:

$$\gamma = \frac{C_p}{C_V}, \quad \rho = \frac{p}{RT}, \quad e = C_V T, \quad C_p - C_V = R, \quad e_0 = e + \frac{\mathbf{u} \cdot \mathbf{u}}{2},$$

where R is the specific gas constant, C_V and C_p are the specific heats and γ the specific heat ratio.

For Newtonian fluids, the viscous stresses are

$$\boldsymbol{\tau} = \mu \left(2\mathbf{S} - \frac{2}{3}(\nabla \cdot \mathbf{u})\mathbf{I} \right), \quad \mathbf{S} = \frac{1}{2} \left(\nabla \mathbf{u} + (\nabla \mathbf{u})^T \right),$$

where μ is the dynamic viscosity, $\mathbf{I}$ is the identity tensor and $\mathbf{S}$ is the rate-of-strain tensor. A Newtonian fluid is a fluid whose viscous stresses are proportional to the shear strain rate. Many common liquids and gases, including the important examples of air and water, can be assumed to be Newtonian. Examples of non-Newtonian fluids are quicksand which stiffens with the increasing shear

strain rate while blood and non-drip paint is less resistant at higher shear strain rates. The fluid in this dissertation is air, thus the assumption of Newtonian fluid is applied.

If the flow has a Mach number Ma < 0.3 it can with good accuracy be approximated as incompressible flow, meaning that the density ρ is assumed to be constant. This also requires that the density does not change significantly for other reasons, such as temperature changes. Assume that the flow is incompressible, the fluid is Newtonian and the body forces $\mathbf{b}$ is known or neglected. Then there are only four unknowns $(\mathbf{u}, p)$ and four equations in the continuity equation (3.1) and momentum equations (3.2). This means that the energy equation is not needed for incompressible flow, simplifying the problem. Should one be interested in the thermal effects of the flow, the energy equation (3.3) can of course be included if desired. Thus, the incompressible Navier-Stokes equations for Newtonian fluids without body forces can be written as:

$$\nabla \cdot \mathbf{u} = 0, \tag{3.4}$$

$$\rho \frac{\partial \mathbf{u}}{\partial t} + \rho \nabla \cdot (\mathbf{u}\mathbf{u}) = -\nabla p + \mu \nabla^2 \mathbf{u}, \tag{3.5}$$

where the following expression for incompressible Newtonian fluids has been used

$$\boldsymbol{\tau} = \mu \left(\nabla \mathbf{u} + (\nabla \mathbf{u})^T \right) = 2\mu \mathbf{S}.$$

Note that the pressure is missing from the continuity equation (3.4). This means that the continuity equation acts as a constraint to the solution. In addition, this means that there is no independent equation for the pressure. This is touched upon again in section 3.3.5.

There are only a few special cases where the Navier-Stokes equations have known analytical solutions. In practice, the only realistic way to achieve solutions of the Navier-Stokes equations is to use computer simulations, or more specifically, Computational Fluid Dynamics (CFD).

3.3.2 Turbulence modelling

The large range of length and time scales of turbulent flows is from a computational view problematic. The resolution and accuracy needed to capture all turbulent scales comes at extreme computational costs except for flows with very low Reynolds numbers. To combat this problem, the turbulence is to a varying degree modelled. The main strategies for dealing with turbulence will here be outlined.

Direct Numerical Simulation

The perhaps conceptually easiest strategy is to simply resolve all turbulent scales all the way down to the Kolmogorov scale. This means that no turbulence model is used, see Figure 3.2. This is called Direct Numerical Simulation (DNS) and is only used for very low Reynolds numbers and mainly in the academic world. It requires very high spatial and temporal resolution as well as high order numerical schemes that have a low numerical dissipation. The computational cost is proportional to Re^3. Using DNS is far too computationally expensive for the problems studied in this dissertation and will remain so for a long time.

Reynolds Averaged Navier-Stokes

To avoid the high costs of DNS, the effects of turbulence can be modelled. In Reynolds Averaged Navier-Stokes (RANS), temporal (or ensemble) averaging is used. The idea is to lower the ambition from resolving everything to getting the right solution in the statistical sense. Any variable f can be decomposed into two parts, an averaged $\overline{f}$ and a fluctuating f', such that $f = \overline{f} + f'$. Only the $\overline{f}$ part is solved for in RANS. The effect of the fluctuations f' is introduced as an unknown called Reynolds stresses in the equations solving for $\overline{f}$. This is typically done by Boussinesq's hypothesis where a turbulent viscosity is added to the normal viscosity of the fluid. All scales of turbulence are taken into account for with the addition of the turbulent viscosity (see also Figure 3.2). The models for how this is done can be fairly elaborate. The common $k-\varepsilon$ family uses two additional transport equations for this purpose alone. The RANS type of modelling is the type of modelling that requires the smallest computational resources. However, it also has the worst accuracy for complex flows. To capture the turbulence interactions with vortex shedding and vortex breakdown properly is central in this dissertation. This makes RANS modelling inadequate.

Large Eddy Simulation

Similarly to RANS, Large Eddy Simulation (LES) also uses averaging or filtering, but in space instead of time. The filtering in LES is performed according to

$$\overline{f} = \int f(x')F_\Delta(x - x')dx',$$

where F_Δ is the LES filter of width Δ. The filtering can be done in physical or spectral space. The idea here is to filter out the small eddies while keeping the large eddies. As already mentioned in section 3.1.2, the smaller turbulent scales exist in the "universal equilibrium range". As the name implies, their behaviour is expected to be universal. This makes them prime target for modelling. The large eddies on the other hand depend on the geometry and flow characteristics and are not modelled. This is illustrated in Figure 3.2. Ideally, parts of the inertial subrange are resolved to ensure that the modelled eddies are well inside the universal equilibrium range. Only a small fraction of the turbulent kinetic energy resides in the modelled part.

The filtering of the smallest length and time scales reduces the resolution requirements compared to DNS. As the filter width Δ gets smaller, the LES solution should tend to the DNS solution. LES places itself in between RANS and DNS both when it comes to accuracy and computational costs. LES captures more aspects of the flow than RANS, but less than DNS. On the other hand, the computational costs are higher than RANS but smaller than DNS. In this dissertation, the accuracy requirements preclude the use of RANS, while the Reynolds numbers makes a DNS simulation far too costly to be possible. Therefore, the LES approach is chosen for the turbulence modelling.

In the incompressible case, the filtered versions of equations (3.4) and (3.5) become

$$\nabla \cdot \overline{\mathbf{u}} = 0, \tag{3.6}$$

$$\rho \frac{\partial \overline{\mathbf{u}}}{\partial t} + \rho \nabla \cdot (\overline{\mathbf{u}\mathbf{u}}) = -\nabla \overline{p} + \mu \nabla^2 \overline{\mathbf{u}}, \tag{3.7}$$

where the overbar indicates filtered quantities. Equation (3.7) is different from (3.5) because $\overline{\mathbf{u}\mathbf{u}} \neq \overline{\mathbf{u}}\,\overline{\mathbf{u}}$. The difference is introduced as an unknown term in the form of the sub-grid stress tensor

$$\boldsymbol{\tau}_{\text{sgs}} = \rho(\overline{\mathbf{u}\mathbf{u}} - \overline{\mathbf{u}}\,\overline{\mathbf{u}}), \tag{3.8}$$

to obtain

$$\rho\frac{\partial\overline{\mathbf{u}}}{\partial t} + \rho\nabla\cdot(\overline{\mathbf{u}}\,\overline{\mathbf{u}}) = -\nabla\overline{p} + \mu\nabla^2\overline{\mathbf{u}} - \nabla\cdot\boldsymbol{\tau}_{\text{sgs}}. \tag{3.9}$$

The equations (3.6) and (3.9) are solved as usual with the sub-grid stress tensor (3.8) calculated from an LES-model (or sub-grid stress model). This is necessary as the $\overline{\mathbf{u}\mathbf{u}}$ term is unknown. Just like RANS models, there are many different LES models. There is also the option of using none at all which means that the numerically introduced dissipation is assumed to be similar to the effect of the unresolved scales. This is called implicit LES or ILES. The ideal LES model should have the following qualities: It should represent the effect of the unresolved scales of turbulence has on the resolved scales of turbulence, dissipate turbulence at the correct rate and take into account for backscatter. In this dissertation, the Smagorinsky model is used which will be outlined below.

The Smagorinsky model

The first LES model to be developed is the Smagorinsky model [43] and it is also one of the simplest. It is based on the Boussinesq's hypothesis already mentioned. In the incompressible case, the model can be summarised by

$$\boldsymbol{\tau}_{\text{sgs}} = -\mu_T\overline{\mathbf{S}}, \quad \overline{\mathbf{S}} = \frac{1}{2}\left(\nabla\overline{\mathbf{u}} + (\nabla\overline{\mathbf{u}})^T\right),$$

where $\overline{\mathbf{S}}$ is the filtered rate-of-strain tensor and μ_T is the turbulent eddy viscosity which is computed as

$$\mu_T = \rho(C_S\Delta)^2\sqrt{2\overline{\mathbf{S}}:\overline{\mathbf{S}}},$$

where C_S is the Smagorinsky constant. The value of C_S is usually set within the range $0.1 < C_S < 0.2$. In the incompressible simulations in this dissertation the OpenFOAM default value of $C_S = (0.094(0.094/1.048)^{1/2})^{1/2} \approx 0.1678$ is used. For compressible flow, the model becomes more complicated, but remains similar in nature. The simplicity of the model makes it popular. The only thing that needs to be specified is the C_S constant, the rest is already known. There are some disadvantages with the model: No backscatter is possible, it can be too dissipative, it overpredicts the viscosity near walls and it does not converge to 0 for laminar flows. There are other models which deal with these disadvantages (and have other disadvantages themselves), but they will not be discussed here. For a comparison of different LES models, the interested reader is referred to [44].

3.3.3 Wall treatment

Most flows of practical interest are wall bounded and have some form of turbulent boundary layer. This is a serious issue in LES simulations. The resolution required for an LES simulation increases in the turbulent boundary layer near walls. The inner layer of the boundary-layer is particularly demanding. According to Piomelli et al. [45], at approximately $\text{Re}_L = 10^6$, where L is the integral length scale, 99 % of the cells used to simulate a boundary-layer flow are used to resolve the inner layer whose thickness is only 10 % of the boundary layer. The share of cells needed in the inner layer also increases with Re_L. Expressed differently; the mesh resolution needed in resolved LES closest to

the wall is nearly as fine as DNS [46]. Clearly, resolving the inner layer with LES is not possible for the Reynolds numbers considered in this dissertation and some kind of modelling is needed. For a more detailed explanation of the higher near wall resolution requirements in LES, see [45].

The main categories of wall-treatments will be discussed briefly. The only model which will be explained in detail is the one used in this dissertation, the `muSgsUSpaldingWallFunction`. For a more complete coverage, the interested reader is referred to [47].

Equilibrium stress models

This class of models tries to use some expression to compute the wall shear stress from the local velocity at the first off-the-wall grid point. This is then fed back to the LES simulation. In a way this can be seen as a wall-stress corrector. If the stresses in the boundary layer are assumed to be in equilibrium (average or instantaneous) this means that the boundary layer should follow the logarithmic law of the wall.

$$u^+ = \frac{u}{u_\tau} = \frac{1}{\kappa}\log y^+ + B, \tag{3.10}$$

where u is the velocity parallel to the wall, u^+ is u in wall units, u_τ is the friction velocity or shear velocity, κ is the von Kármán constant, y^+ is the distance y to the wall in wall units ($y^+ = (y u_\tau \rho)/\mu$) and B is a constant. For (3.10) to be applicable, the first grid point must be in the so called log-law region, i.e. far enough from the wall that viscous effects are negligible. To ensure this, the first grid point of the wall should be placed at $y^+ > 30$.

In OpenFOAM (version 2.1.1), there exists a model called `muSgsUSpaldingWallFunction` in the compressible case and `nuSgsUSpaldingWallFunction` in the incompressible case. This model uses the more universal velocity profile, Spalding's law [48]:

$$y^+ = u^+ + \frac{1}{E}\left(e^{\kappa u^+} - 1 - \frac{\kappa u^+}{1!} - \frac{(\kappa u^+)^2}{2!} - \frac{(\kappa u^+)^3}{3!}\right), \tag{3.11}$$

where κ and E are constants with the default values of $\kappa = 0.41$ and $E = 9.8$. The values of y^+ and u^+ are computed by inserting the known values of y and u next to the wall into $y^+ = (y u_\tau \rho)/\mu$ and $u^+ = u/u_\tau$, respectively. Then (3.11) is iterated using the Newton-Raphson method to determine the value of u_τ. The following relations that apply for the wall shear stress τ_w

$$\tau_w = (\mu + \mu_T)\left(\frac{\partial u}{\partial y}\right)_{y=0} = u_\tau^2 \rho,$$

is then used to obtain the turbulent viscosity at the wall

$$\mu_T = \frac{u_\tau^2 \rho}{\left(\frac{\partial u}{\partial y}\right)_{y=0}} - \mu.$$

Using Spalding's law instead of the log-law (3.10) removes the restriction of $y^+ > 30$. If the boundary layer is well resolved in the other aspects, the simulation should converge to a DNS boundary layer solution as the near-wall cells are refined. This does not force a change of wall-treatment when $y^+ < 30$ which would have been the case if the log-law would have been used.

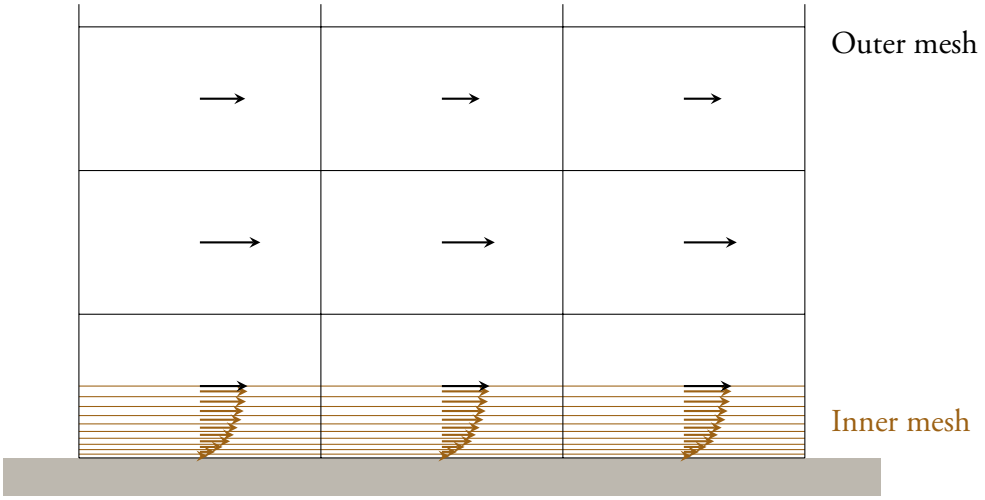

Figure 3.6: Inner and outer mesh for the two-layer model.

Two-layer models

In the two-layer models two separate grids are used. There is a coarser outer mesh that takes care of the flow away from the wall, and a mesh inside the cell of the coarse mesh that is closest to the wall. This second mesh is much refined in the wall-normal direction, see Figure 3.6. The standard filtered LES equations are solved on the coarser mesh and simplified transport equations called boundary layer equations are solved in the finer inner mesh. The inner mesh is solved with a no-slip BC next to the wall and with the velocity from the coarser mesh in the upper interface. The wall-stress is then integrated over the finer mesh and is used as BC for the coarser outer mesh. According to [47] the two-layer models only increase the cost of an LES calculation by 20 to 30 % compared to the use of wall functions (equilibrium stress models). The two-layer models have the advantage when compared to equilibrium models of being more accurate in situations where the equilibrium assumptions do not hold. On the other hand, in situations where assumptions of the simplified equations used in the near wall mesh are invalid, the accuracy will suffer. The two-layer models have an obvious drawback. It requires a second mesh that matches the outer mesh along all walls that the model is applied to. Also, dealing with two simulations in one is more complex.

Detached eddy simulation

Detached Eddy Simulation (DES) is a hybrid between LES and RANS. Similarly to the two-layer model the simulation is divided into two parts where LES is used in the outer flow away from the walls and RANS is used near walls. However, in contrast to two-layer models, the same mesh is used forming one single domain. The first DES model was proposed in 1997 by Spalart et al. [49] making it a fairly recent model. The use of RANS in the near wall region is a much more advanced treatment than the other models discussed here, enabling greater accuracy in the near wall region. It also enables the use of RANS quality meshes near the wall. That is, the wall-normal resolution is high, but the streamwise resolution can be much coarser than in LES. It has achieved great success in many areas and there is a very active development of new DES methods. Nevertheless, the DES concept has its disadvantages.

The first DES model [49] uses the Spalart-Allmaras (S-A) one-equation eddy viscosity model [50] as the RANS model. In the LES mode, the S-A model is similar to the Smagorinsky model. The model includes a term d that depends on the distance to the closest wall y_w in the RANS zone and on the largest cell dimension Δ_{DES} in the LES zone. This is achieved by $d = \min(y_w, \Delta_{\mathrm{DES}})$. This also means that the relation between y_w and Δ_{DES} determines if the cell is in the RANS or LES zone. Close to the wall y_w is smaller than Δ_{DES} so the RANS model is chosen and vice versa far from the wall. This means that when the mesh is refined near the wall, the RANS zone will diminish. This is not always good as it is desired that the RANS model takes care of the near wall region. In fact, this can cause so called grid-induced separation where the flow separates due to grid refinement. This is counter-intuitive as one typically likes to be able to improve the solution by refining the grid until grid independence is reached. Here, the solution can actually become worse as the mesh is refined. This has been addressed in several variants, perhaps most notably the Delayed Detached Eddy Simulation (DDES) [51]. Still, the user must be careful with the mesh generation.

Another issue with DES is the log-layer mismatch. The RANS solution does not need to match the LES solution in the interface between the two. This causes a more or less sudden jump in velocity between the regions. Mesh refining appears to only move the point of mismatch. This is discussed in [52] when DES is used as a wall model to channel flow.

The strength of DES is in separated flows, such as the flow around a cylinder. In this case there is a boundary layer mainly on the upstream half of the cylinder. Any vortices formed in this boundary layer will be overpowered by the turbulence from the separation. However, there is an issue highlighted by de Villiers [47] when the vortices formed at separation are affected by the upstream boundary layer. The RANS near wall solution should in theory reduce to a steady RANS solution with no resolved eddies in it. The RANS properties of the boundary layer should be fine; it is just that any resolved turbulence is suppressed. This is not an issue in the cylinder case described above. Clearly, if the wall-attached eddies have a strong effect on the eddies caused by separation, this is an issue. This was determined by de Villiers when applying it to an asymmetric plane diffuser [47]. In paper A, it is found that the turbulence in the incoming boundary layer has an important effect on the rate of break-up of the Kelvin-Helmholtz (K-H) vortices shed from the step edge of the backward-facing step. A lack of turbulence in the incoming boundary layer decreases the K-H vortices break-up rate, increasing the pressure fluctuations on the downstream surface. For this reason DES is not very well suited for this kind of problem. For a review on DES methods, see [52].

3.3.4 Numerical discretisation

Within the subject of Computational Fluid Dynamics (CFD) there exist several discretisation strategies. The three main categories are Finite Differences (FD), Finite Volume (FV) and Finite Elements (FE). Finite differences is the oldest of the three. It is often used on Cartesian grids or structured grids that have a high regularity. Exploiting such properties gives fast codes and codes with a small memory footprint. They are simple and allow the use of high order schemes resulting in high accuracy. However, the grid requirements make it difficult to handle complex geometries reducing its flexibility. The combination of high accuracy and low flexibility makes it mainly popular in the academic world for problems with simple geometries.

Despite the popularity of the finite element method in many engineering fields such as solid mechanics and structural dynamics, it has traditionally not been extensively used in fluid mechanics.

The FE-method can use high order accuracy and handle arbitrary geometries well. But there are two disadvantages that have held it back. The conservation properties are very important in CFD and FE-methods have traditionally been unable to conserve mass. Also, FE-methods tend to use more computational resources than FV and FD methods due its higher order nature. It turns out that a lower order method with more grid points is often preferable in CFD. Nevertheless, FE based CFD appears to be on the rise with FE based CFD modules being integrated into large FE software packages for structural analysis.

The finite volume discretisation is the most common discretisation strategy employed in CFD. The domain is divided into a finite number of control volumes and the discretisation is based on the conservation of quantities in each control volume. The main advantages are that quantities are conserved and that complex geometries can be easily accommodated. However, there is one disadvantage against both FD and FE methods: It is difficult to develop higher order interpolation schemes.

The filtered Navier-Stokes equations with the corresponding sub-grid stress models discussed in previous sections results in many different terms that require discretisation. Instead of addressing every term specifically, the following transport equation for the generic variable ϕ (which may be a scalar, vector or tensor) is studied,

$$\underbrace{\frac{\partial}{\partial t}\int_V \rho\phi \mathrm{d}V}_{\text{Time derivative}} + \underbrace{\int_V \nabla\cdot(\rho\mathbf{u}\phi)\mathrm{d}V}_{\text{Convection}} - \underbrace{\int_V \nabla\cdot(\rho\Gamma\nabla\phi)\mathrm{d}V}_{\text{Diffusion}} = 0, \tag{3.12}$$

where Γ is the diffusivity coefficient.

Spatial discretisation

In the finite volume method, the entire computational domain is divided into control volumes, or cells. The cells do not overlap and can have an arbitrary number of faces (sides) as long as the faces are convex, see Figure 3.7. The mesh can be structured or unstructured. The quantities of interest are mainly stored at the cell centre P and are co-located, i.e. all quantities share the same cells. Here, the discretisation of some general terms will be illustrated, for a more complete derivation, see the work by Jasak [53].

In the FV-method, the quantities of interest are integrated over the cell. With ϕ being the variable of interest, this means

$$\int_{V_P} \phi(\mathbf{x})\mathrm{d}V = \phi_P V_P, \tag{3.13}$$

where V_P is the cell volume and ϕ_P is ϕ at the cell centre P. For the divergence operator this gives

$$\int_{V_P} \nabla\cdot\phi\mathrm{d}V = \int_{\partial V_P} \phi\cdot\mathrm{d}\mathbf{A} = \sum_f \left(\int_f \phi\cdot\mathrm{d}\mathbf{A}\right) = \sum_f \phi_f\cdot\mathbf{A}, \tag{3.14}$$

where $\mathbf{A}$ is the outward pointing surface area vector, f is the (flat) face surface and ϕ_f is the value of ϕ_f on the surface. The value of ϕ_f needs to be determined from some form of interpolation which will be described later.

Applying (3.13) and (3.14) to the generic convection term in (3.12) gives

$$\int_{V_P} \nabla\cdot(\rho\mathbf{u}\phi)\mathrm{d}V = \sum_f (\rho\mathbf{u}\phi)_f\cdot\mathbf{A} = \sum_f \phi_f(\rho\mathbf{u})_f\cdot\mathbf{A} = \sum_f \phi_f F_f, \tag{3.15}$$

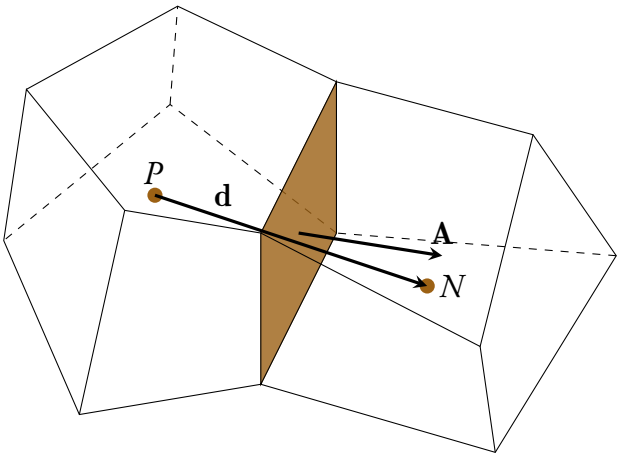

Figure 3.7: Control volume, or cell, for the finite volume discretisation.

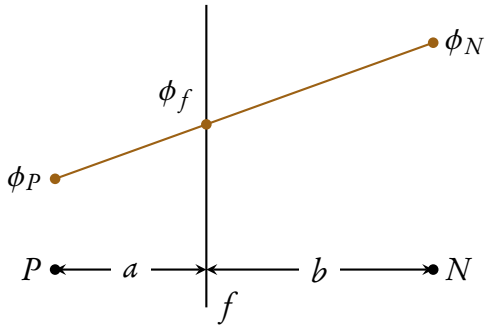

Figure 3.8: Face interpolation.

where F_f is the mass flux through the face f, $F_f = (\rho \mathbf{u}_f) \cdot \mathbf{A}$. In the incompressible case where the density is constant, the following condition on the mass flux must be enforced,

$$\sum_f F_f = 0.$$

The term ϕ_f, the value of ϕ at the faces, in equations (3.14) and (3.15) needs to be determined as only the cell centre values are stored. This can be done via linear interpolation according to

$$\phi_f = \alpha \phi_P + (1 - \alpha)\phi_N,$$

where ϕ_P is the value in the present cell P and ϕ_N is the value in the neighbouring cell N. α is the ratio between the distance from P to f and P to N as given by $\alpha = a/b$ where a and b are defined as illustrated in Figure 3.8. This is known as Central Differencing (CD) and is second order accurate on structured as well as unstructured meshes. There is a serious drawback of the CD scheme, as it can cause unphysical oscillations when the convection term dominates. If the oscillations are severe, the solution may even diverge.

Instead of interpolating the value ϕ_f on both ϕ_P and ϕ_N as is done in CD, Upwind Differencing (UD) only uses the upwind, or upstream, value. This means that the scheme depends on the direction of the flux. The first order UD scheme is

$$\phi_f = \begin{cases} \phi_P & F \geq 0 \\ \phi_N & F < 0 \end{cases}.$$

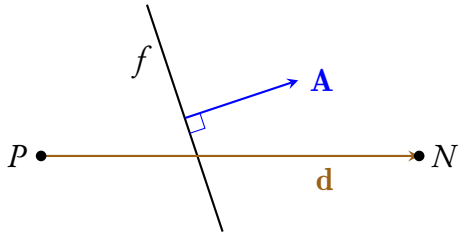

Figure 3.9: A non-orthogonal mesh.

The problem with upwind schemes is that they introduce numerical viscosity into the system. This does increase the stability of the solution compared to the CD schemes, but the stability comes with reduced accuracy. The extra viscosity is undesired as it not only reduces the accuracy but can also dissipate turbulence at a higher rate than what would be physical.

For the important convection of velocity term $\nabla \cdot (\rho \mathbf{uu})$, the LUST (Linear-Upwind Stabilised Transport) scheme is used in this dissertation. It uses a blend of 75 % CD and 25 % linear-upwind differencing (second order variation of the UD scheme above). The linear-upwind stabilises the CD scheme while maintaining second order behaviour and is particularly successful for LES/DES in external aerodynamics of vehicles according to the OpenFOAM foundation [42]. For the other convection terms in the compressible case, the Gamma scheme is used. The Gamma scheme [54] is a blended scheme where CD is normally used in most of the domain. However, CD can become unbounded. When this occurs, the CD is blended with some UD for stability. In severe unboundedness the scheme uses only UD. There is a parameter that can be specified which affects how much blending should be used and when it should be used. Essentially, this parameter specifies how the scheme should prioritise between accuracy and stability. In this dissertation, the parameter is set to maximum stability. For further details, see [54].

For diffusion term in (3.12), the same basic procedure with (3.13) gives

$$\int_{V_P} \nabla \cdot (\rho \Gamma \nabla \phi) \mathrm{d}V = \sum_f (\rho \Gamma \nabla \phi)_f \cdot \mathbf{A} = \sum_f (\rho \Gamma)_f (\nabla \phi)_f \cdot \mathbf{A}. \tag{3.16}$$

If the mesh is orthogonal, i.e. the vectors $\mathbf{d}$ and $\mathbf{A}$ in Figure 3.9 are parallel, the face gradient term in (3.16) may be expressed as

$$(\nabla \phi)_f \cdot \mathbf{A} = \frac{\phi_N - \phi_P}{|\mathbf{d}|} |\mathbf{A}|. \tag{3.17}$$

If the mesh is not orthogonal, which is the norm rather than the exception in real applications, (3.17) needs to be modified to maintain second order accuracy as follows

$$(\nabla \phi)_f \cdot \mathbf{A} = \frac{\phi_N - \phi_P}{|\mathbf{d}|} |\mathbf{A}| + \mathbf{k} \cdot (\nabla \phi)_f,$$

where the second term is the non-orthogonal correction. The differential form, (3.12), of the diffusion term has bounded behaviour. However, boundedness is only preserved on orthogonal meshes as the non-orthogonal correction potentially introduces unboundedness if non-orthogonality is high in the mesh. For severely non-orthogonal meshes, it may therefore be desired to limit or eliminate the correction. In this dissertation, the non-orthogonality is deemed to be within acceptable limits

and the non-orthogonal correction is applied. The details of the non-orthogonal correction will not be explored here. Instead the interested reader is referred to Jasak [53] which discusses several approaches for the non-orthogonal correction.

To summarise the spatial discretisation, (3.13), (3.15) and (3.16) are plugged into the generic transport equation in (3.12) to obtain

$$\left(\frac{\partial \phi}{\partial t}\right)_P V_P + \sum_f \phi_f F_f - \sum_f (\rho\Gamma)_f (\nabla\phi)_f \cdot \mathbf{A} = 0. \tag{3.18}$$

The remaining terms in the governing equations, gradient terms, have in this dissertation had CD schemes applied to them.

Time discretisation

As the simulations carried out in this dissertation are transient, the spatially discretised generic transport equation in (3.18) needs to be integrated in time as

$$\int_t^{t+\Delta t} \left(\left(\frac{\partial(\rho\phi)}{\partial t}\right)_P V_P + \sum_f \phi_f F_f - \sum_f (\rho\Gamma)_f (\nabla\phi)_f \cdot \mathbf{A} \right) \mathrm{d}t = 0, \tag{3.19}$$

where Δt is the length of one time step. Therefore some time discretisation scheme is needed. In this dissertation two approaches are used. In paper A, the incompressible case, second order backward differencing is used, while in paper B, a blend of time centred Crank-Nicholson and Euler implicit differencing is used. Both will now be outlined and discussed.

Crank-Nicholson uses the following expressions to calculate the time derivative and time integral of ϕ

$$\left(\frac{\partial(\rho\phi)}{\partial t}\right)_P = \frac{\rho_P^n \phi_P^n - \rho_P^{n-1}\phi_P^{n-1}}{\Delta t}, \tag{3.20}$$

$$\int_t^{t+\Delta t} \phi(t)\mathrm{d}t = \frac{1}{2}(\phi^n + \phi^{n-1})\Delta t, \tag{3.21}$$

where $\phi^n = \phi(t + \Delta t)$, or the new time step, and $\phi^{n-1} = \phi(t)$, or the current time step. Inserting (3.20) and (3.21) into (3.19) gives

$$\frac{\rho_P^n \phi_P^n - \rho_P^{n-1}\phi_P^{n-1}}{\Delta t} V_P + \frac{1}{2}\left(\sum_f \phi_f F_f - \sum_f (\rho\Gamma)_f (\nabla\phi)_f \cdot \mathbf{A}\right)^n + \frac{1}{2}\left(\sum_f \phi_f F_f - \sum_f (\rho\Gamma)_f (\nabla\phi)_f \cdot \mathbf{A}\right)^{n-1} = 0.$$

This means that the face and cell centred values of ϕ and $\nabla\phi$ as well as the convective and diffusive fluxes for both the current and new times are required. Also, the flux and non-orthogonal correction of the diffusion term must be computed for the new time which means that the Crank-Nicholson scheme requires inner iterations for each time step. The Crank-Nicholson scheme is a second order

accurate scheme. The scheme is used in paper B blended with the Euler implicit method outlined below.

The following methods neglect the variation of ϕ_f and $(\nabla\phi)_f$ in time, leaving only the time derivative to be handled by the time discretisation scheme. If (3.20) is used for the time derivative, (3.19) becomes

$$\frac{\rho_P^n\phi_P^n - \rho_P^{n-1}\phi_P^{n-1}}{\Delta t}V_P + \left(\sum_f \phi_f F_f - \sum_f (\rho\Gamma)_f(\nabla\phi)_f \cdot \mathbf{A}\right)^n = 0,$$

which is the Euler implicit method. It is only first order accurate. In paper B, initial tests with the Crank-Nicholson method produced unphysical oscillations. To supress the oscillations, the Crank-Nicholson scheme was blended with the Euler implicit method.

The time discretisation scheme can be made second order accurate while still neglecting the variation of ϕ_f and $(\nabla\phi)_f$ in time. This is done by raising the order of discretisation used for the time derivative. Backward differencing in time uses

$$\left(\frac{\partial(\rho\phi)}{\partial t}\right)_P = \frac{\frac{3}{2}\rho_P^n\phi_P^n - 2\rho_P^{n-1}\phi_P^{n-1} + \frac{1}{2}\rho_P^{n-2}\phi_P^{n-2}}{\Delta t},$$

instead of (3.20), turning (3.19) into

$$\frac{\frac{3}{2}\rho_P^n\phi_P^n - 2\rho_P^{n-1}\phi_P^{n-1} + \frac{1}{2}\rho_P^{n-2}\phi_P^{n-2}}{\Delta t}V_P + \left(\sum_f \phi_f F_f - \sum_f (\rho\Gamma)_f(\nabla\phi)_f \cdot \mathbf{A}\right)^n = 0,$$

This scheme is less computationally expensive than the Crank-Nicholson scheme and has lower memory overhead while both schemes are second order accurate. However, the truncation error is four times larger in the backward differencing scheme [53], so there is a trade-off. The backward differencing scheme is used in paper A.

3.3.5 Solver algorithms

The main solution algorithm used in this dissertation is the Pressure Implicit with Splitting of Operators (PISO) algorithm proposed by Issa [55]. The algorithm will only be briefly outlined. The basic idea of the PISO algorithm is that the pressure-velocity system of the Navier-Stokes equations has two complex coupling terms: The non-linear convection term and the linear pressure-velocity coupling. For small time-steps, the pressure velocity coupling should be the stronger of the two. Therefore, develop a pressure equation that is used to perform a few repeated number of pressure corrections without updating the velocities via the momentum equation. For the derivation of the pressure equation and other details, see [47, 53]. For incompressible flow, the PISO algorithm is roughly as follows:

1. Update all derived (turbulent) quantities from the previous values of $\overline{\mathbf{u}}$, F and $\overline{p}$.
2. Solve the discretised momentum equations for the velocity using the previous values for F and $\overline{p}$.
3. Calculate the face fluxes using the new approximate velocity field while maintaining continuity.

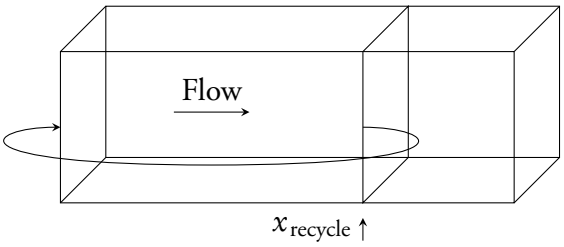

Figure 3.10: Description of the computational domain of the precursor simulation.

4. Solve the pressure equation using the new velocities.
5. If non-orthogonality correction as described in section 3.3.4 is used, perform the correction here.
6. Correct the approximated velocity field with corrected pressures and repeat from step 3 with the new approximated velocity until the desired number of correction steps has been performed.

For compressible flows, the algorithm is similar. In step 2, the energy equation (3.3) is also solved. There are also density correctors at appropriate points in the algorithm.

The solution method of the linear systems of equations in the algorithm above is needed. With the exception of the pressure equation in the incompressible case in paper A, the Diagonal Incomplete LU Preconditioned BiConjugate Gradient (DILUPBiCG) strategy was used. For the incompressible case in paper A, the pressure equation was solved using the Geometric-Algebraic Multi-Grid (GAMG) solver. This reduced the needed total computational cost considerably. However, the parallel scalability of GAMG was lower. It was possible to achieve a solution faster by using DILUPBiCG, but the total core-hours spent was much larger and it was therefore decided to use the GAMG solver. Using the GAMG solver in the compressible case in paper B was not beneficial at all and the DILUPBiCG method was used.

3.3.6 Precursor inlet boundary condition

Paper A uses a ramped backward-facing step as a model problem. Initially, a prescribed velocity profile taken from the measurements in [56], without any fluctuations was used as inlet boundary condition (BC). This resulted in a laminar boundary layer at the step edge. The interaction between the incoming turbulence in the boundary layer affects the break-up of the K-H vortices shed from the step edge (for the general characteristics of backward-facing step flow, see section 3.2.2). The lack of turbulence in the boundary layer resulted in an overprediction of the downstream surface pressure fluctation intensity. While not studying the surface pressure fluctuations specifically, this effect was demonstrated by Aider et al. [57]. They also demonstrated that simple synthetic turbulence-generating inlet BCs are also insufficient as the turbulence tend not to survive long enough distances. Instead, high quality turbulence is needed at the inlet.

A method for generating a high quality turbulent boundary layer of a desired thickness has been developed by Lund et al. [58] and works as follows: An auxiliary simulation, called precursor simulation, is used. The sole purpose of the precursor simulation is to generate the inlet BC for the main simulation. The precursor simulation contains flow over a flat plate. It generates its own inlet BC by mapping the re-scaled velocity field from a point downstream x_{recycle} back to the inlet (of

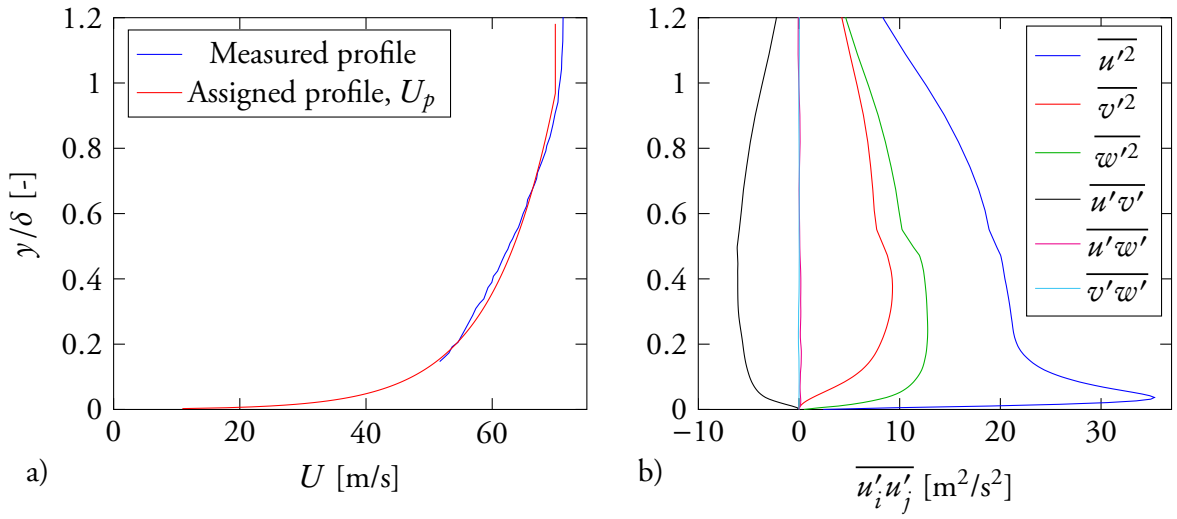

Figure 3.11: a) Mean streamwise velocity profile used for scaling purposes in the percursor simulation. b) Mean Reynolds stress distribution in the inlet BC of the main simulation.

the precursor simulation). This is illustrated in Figure 3.10. Remember that the thickness of the boundary layer δ over a flat plate grows as it travels downstream (see section 3.2.1). If the velocity was not re-scaled, δ would keep growing as time passed in the simulation. The purpose of the re-scaling is to keep δ at the desired value.

Unfortunately, when the work on paper A was carried out, this BC was not implemented in OpenFOAM. However, there existed a similar BC for channel flow. This BC does not perform the described scaling as there purpose is to generate a similar BC for fully developed channel flow. Due to time constraints, a simplified version of the Lund BC was implemented. The difference lies in the scaling. In the version implemented by the author an assumed, or prescribed, mean streamwise velocity profile U_p is used.

$$U_p = A\log(y) + B,$$

where A and B was fitted to the measured mean streamwise velocity profile when there was no obstacle in the wind tunnel in [56]. Both the measured and the assigned profile U_p is shown in Figure 3.11a. The scaling is done as

$$u_{\text{scaled}} = \frac{U_p}{\langle u_{\text{recycle}} \rangle} u_{\text{recycle}},$$

where u_{recycle} is the streamwise velocity component sampled at the downstream location x_{recycle} as indicated in Figure 3.10, $\langle u_{\text{recycle}} \rangle$ is the spanwise mean of u_{recycle} for one row of cells, and u_{scaled} is the scaled result that is recycled back to the inlet of the precursor simulation. Neither the wall-normal nor the spanwise velocity component is scaled. The resulting Reynolds stresses of the inlet BC generated by the method that is used in this work is given in Figure 3.11b.

This method does not preserve the physical properties of the turbulent boundary-layer to the same extent as the method developed by Lund et al. [58]. Nevertheless, since the computational effort to fully resolve the turbulent boundary layer without the aid of wall functions would have been too large, it was deemed that this implementation should still provide turbulence in the boundary

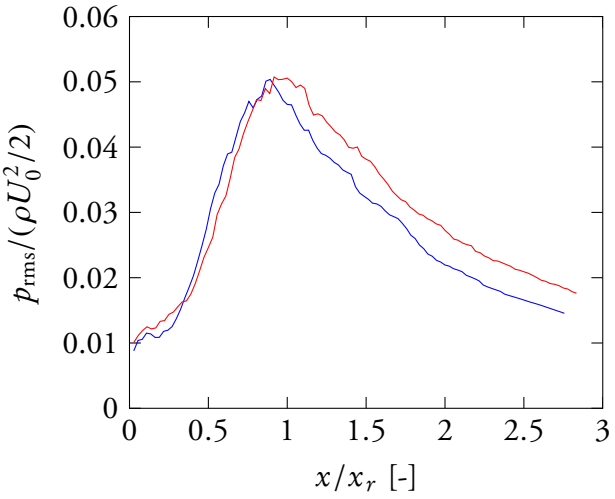

Figure 3.12: Streamwise distribution of r.m.s. fluctuating pressure behind the step in paper A. Curves: (—) is the simplified inlet BC implemented by the author and (—) is the full Lund BC as implemented by Hodara.

layer that is realistic enough to create useful results. After the work in paper A was carried out, another researcher unrelated to this work has implemented the Lund BC in OpenFOAM and kindly provided the implementation for comparison[2]. Figure 3.12 gives a preliminary comparison between both inlet BC methods on the streamwise distribution on the p_{rms} value downstream of the step in paper A. It appears that both methods produce similar end results.

[2]Joachim Hodara at Georgia Institute of Technology is gratefuly acknowledged for sharing his implementation of the Lund inlet BC.

4 Structural response

This chapter discusses methods used to predict the vibration of thin panel structures exposed to a pressure load. In particular, the method used in paper A will be described. This method is a time domain method that uses modal reduction and Newmark's time stepping algorithm. There are other possibilities on how to perform the structural response prediction. One such method is used in the ACOUFAT project [2, 24]. Their method uses the frequency domain instead of the time domain used here. As load input they use the power spectral densities (PSD) and the complex cross-spectral densities between different spatial points of the load. The results in [2, 24] indicates that the method is successful. The main focus in this dissertation is to predict the load rather than focusing on the response prediction. Therefore, the more readily available method described in this chapter was chosen. For future work, there is clearly the possibility to explore the frequency domain method employed in [2, 24] and possibly other methods as well.

4.1 Plate theory

The basic design of an aircraft surface skin panel structure is illustrated in Figure 2.2. The thin outer surface can be made of aluminium or composite material that is attached to an array of stringers and ribs. Figure 2.2 illustrates the panel design used in the ACOUFAT project [24], which was flat. As aircraft generally have a cylindrical shape, the skin surface panels of real aircraft are curved. In paper A, the response of a flat rectangular aluminium sheet attached with many fasteners along its edges is investigated. This sheet represents the outer skin surface of an aircraft.

The thin sheets forming the skin surface panel structure lends itself very well to the use of plate theory. There are two plate theories that have a wide-spread adoption: the Kirchhoff-Love theory and the Mindlin-Reissner theory. The Kirchhoff-Love theory uses the following assumptions:

1. The plate is thin.
2. The plate is linear-elastic.
3. Deflections and slopes are small.
4. Straight lines normal to the middle surface before deformation remain straight and normal to that surface after deformation.
5. The normal stresses in the direction transverse to the plate can be disregarded.

The equivalent assumptions are made in the Euler-Bernoulli beam theory, which the Kirchhoff-Love plate theory can be seen as an extension of. The Mindlin-Reissner is a more complex plate theory that handles thick plates by taking into account the shear deformations through the thickness of the plate. This is done by relaxing assumption four into: Straight lines normal to the middle surface before deformation remain straight. The analogous beam theory to the Mindlin-Reissner plate theory is the

Timoshenko beam theory. More on plate theory may be found in [59, 60]. The aluminium sheet in paper A, as well as many outer skin surfaces on aircraft, are sufficiently thin for the simpler Kirchhoff-Love theory, which is therefore used. Also, the deflections are small enough for the aluminium sheet in paper A. As discussed in section 2.3, this is not necessarily the case for all surface skin panels on aircraft in general.

4.2 Finite Element Method

In this dissertation, a Finite Element (FE) formulation of the Kirchhoff-Love plate theory is used. The FE software used is the in house open-source software package CALFEM [61] which includes a Kirchhoff-Love plate element. The specific element routine used in paper A, however, is an unpublished routine that extends the published plate element to support a consistent mass matrix and is isoparametric. Since all elements in paper A has its edges along the coordinate axis and the computational mesh is fine, similar results should be obtained if the published plate element is used together with a lumped mass matrix.

It is not necessary to use the FE method in order to use plate theory. The Kirchhoff-Love plate theory can be used to develop simple analytical single degree-of-freedom (SDOF) models and multi degree-of-freedom (MDOF) models directly. This is done and used in the ESDU design guidelines [1]. In paper A, the FE method was chosen for two reasons. First, the complex time and spatial distribution of the load extracted from the CFD-simulation can easily be applied to the structure with the FE method. Second, the FE method is a very powerful general tool that can handle complex shapes and materials as well as non-linear response as discussed in chapter 2. Even though the aluminium sheet in paper A is a simple structure, it is desired to investigate it with more powerful and general methods.

The FE discretisation produces the following system of equations

$$\mathbf{M}\ddot{\mathbf{a}}(t) + \mathbf{C}\dot{\mathbf{a}}(t) + \mathbf{K}\mathbf{a}(t) = \mathbf{p}(t), \tag{4.1}$$

where $\mathbf{M}$ is the mass matrix, $\mathbf{C}$ is the damping matrix, $\mathbf{K}$ is the stiffness matrix, $\mathbf{a}(t)$ is the nodal displacements vector, $\mathbf{p}(t)$ is the pressure load vector and the dot $\dot{\mathbf{a}}(t)$ indicates time derivative. The derivations and methods used to form these matrices are not covered here as it would take considerable space to present. In particular the FE-formulation of the plate theory is rather lengthy. The interested reader is instead directed to a textbook on the FE-method such as [62] or [63] and the CALFEM manual [61].

4.3 Modal reduction

If the structure is lightly damped, a reduced order model can be derived as follows. First study the free vibration of the undamped system ($\mathbf{C} = \mathbf{0}, \mathbf{p}(t) = \mathbf{0}$) with n degrees-of-freedom.

$$\mathbf{M}\ddot{\mathbf{a}}(t) + \mathbf{K}\mathbf{a}(t) = \mathbf{0}. \tag{4.2}$$

Assume a solution on the form

$$\mathbf{a}(t) = \mathbf{\Phi}\mathbf{q}(t), \tag{4.3}$$

$$\mathbf{\Phi} = [\boldsymbol{\phi}_1 \cdots \boldsymbol{\phi}_n], \quad \mathbf{q}(t) = [q_1(t) \cdots q_n(t)]^T, \quad q_n(t) = A_n \cos(\omega_n t) + B_n \sin(\omega_n t),$$

Note that $\boldsymbol{\phi}_n$ are vectors. This gives

$$\ddot{\mathbf{a}}(t) = -\omega_n^2 \boldsymbol{\Phi}\mathbf{q}(t) = -\omega_n^2 \mathbf{a}(t).$$

Inserting this into (4.2) gives

$$(\mathbf{K} - \omega_n^2 \mathbf{M})\boldsymbol{\Phi}\mathbf{q}(t) = \mathbf{0}.$$

If $\mathbf{q}(t) = \mathbf{0}$, then $\mathbf{u}(t) = \mathbf{0}$, i.e. no motion. Since this condition is fairly uninteresting, assume $\mathbf{q}(t) \neq \mathbf{0}$, which gives

$$(\mathbf{K} - \omega_n^2 \mathbf{M})\boldsymbol{\Phi} = \mathbf{0}. \tag{4.4}$$

Once again, disregard $\boldsymbol{\Phi} = \mathbf{0}$ as it implies no motion. The remainder has non-trivial solutions when

$$\det(\mathbf{K} - \omega_n^2 \mathbf{M}) = 0. \tag{4.5}$$

Solving the eigenvalue problem (4.5) gives n eigenfrequencies $\omega_1, \ldots, \omega_n$. If the eigenfrequencies are inserted into (4.4), then the corresponding eigenmodes $\boldsymbol{\phi}_1, \ldots, \boldsymbol{\phi}_n$ can be computed.

The obtained eigenfrequencies and eigenmodes can be used to transform the original system of equations (4.1) into

$$\tilde{\mathbf{M}}\ddot{\mathbf{q}}(t) + \tilde{\mathbf{C}}\dot{\mathbf{q}}(t) + \tilde{\mathbf{K}}\mathbf{q}(t) = \tilde{\mathbf{p}}(t), \tag{4.6}$$

$$\tilde{\mathbf{M}} = \boldsymbol{\Phi}^T \mathbf{M}\boldsymbol{\Phi}, \quad \tilde{\mathbf{C}} = \boldsymbol{\Phi}^T \mathbf{C}\boldsymbol{\Phi}, \quad \tilde{\mathbf{K}} = \boldsymbol{\Phi}^T \mathbf{K}\boldsymbol{\Phi}, \quad \tilde{\mathbf{p}}(t) = \boldsymbol{\Phi}^T \mathbf{p}(t).$$

The $\tilde{\mathbf{M}}$ and $\tilde{\mathbf{K}}$ matrices are now diagonal. If a diagonal $\tilde{\mathbf{C}}$ is provided as well, the system of equations in (4.6) becomes uncoupled. With a diagonal $\tilde{\mathbf{C}}$, the ith row of (4.6) can be rewritten in standard form

$$\ddot{q}_i(t) + 2\zeta_i \omega_i \dot{q}_i(t) + \omega_i^2 q_i(t) = \frac{p_i(t)}{m_i}, \tag{4.7}$$

where ζ_i and m_i is the diagonal element of the ith row of $\tilde{\mathbf{C}}$ and $\tilde{\mathbf{M}}$, respectively, and p_i is the ith row of $\tilde{\mathbf{p}}$. ζ_i is known as the modal damping ratio. The q_i determined from (4.7) can be plugged back into (4.3) to determine the displacements.

Solving n uncoupled equations is much faster than solving n coupled equations. On the other hand, the eigenfrequencies and the eigenmodes have to be determined first. For many kinds of structures, the response is dominated by just a few modes that have the lowest eigenfrequencies. This is the case for the aluminium sheet in paper A. In such cases, the contributions of only the modes with lowest frequency need to be considered, reducing the number of equations in (4.6). Therefore, the method described in this section is used in paper A. The decoupled equations in (4.7) are solved iteratively by the time-stepping method developed by Newmark [64]. The values of the two parameters in Newmark's method used are $\gamma = 1/2$ and $\beta = 1/4$, which corresponds to the average acceleration method. For a more modern and convenient description of Newmark's method, as well as a more detailed treatment of modal reduction and the dynamics of structures, see [65].

4.4 Damping

The damping of a structure is the effect of energy loss via dissipation. Without damping, a structure that is excited by a load at the resonance frequency would theoretically always reach infinite displacements unless the source of loading was removed. The damping increase stability, both in

the physical and the computational world. The sources of the dissipation can be many. For example damping can occur inside the material of the structure due to its microstructure. It can also be caused by friction in joints and due to contact near bolts and screws.

There are accurate and simple ways to obtain the mass $\mathbf{M}$ and stiffness $\mathbf{K}$ matrices for many structures. For the aluminium sheet in paper A, it is enough to know the material properties and the geometry of the sheet. Damping on the other hand, is very difficult to estimate. In this dissertation the modal formulation is used. Therefore one damping value is needed for each of the included modes as demonstrated by (4.7). These values were obtained from the measurements that are used for comparison in paper A [66] by using the half-power bandwidth method. In paper A, the first few modes were estimated using the half-power bandwidth method, while higher modes were given a fixed value of 1 %.

4.5 Fluid-structure coupling

So far the motion of the fluid and the structure has been dealt with separately in this dissertation. But as a consequence of Newton's third law, the fluid and the structure are coupled; the fluid exert force on the structure, and vice versa. This is possible to handle with various simulation tools and is called Fluid-Structure Interaction (FSI). In this dissertation some of the coupling is neglected. The FE structural response simulation dealt with in this chapter uses the load extracted from the CFD simulation of the fluid. The resulting vibration of the structure, however, is not taken into consideration in the simulation of the fluid. The fluid simulation does take the presence of the rigid structure into consideration by wall BC:s, but not the vibration of the structure. The motivation for this is that the effect on the flow would have been negligible. This means that the problem is only one way coupled. The data from the simulation of the fluid is sent to the simulation of the structure, but not vice versa.

The coupling method was chosen for simplicity. The reason for this is that the main focus of the dissertation has been in the load prediction rather than investigating different coupling schemes. The pressure load is extracted as the pressure value directly from the CFD-simulation. To avoid the need for an interpolation algorithm, matching meshes are used at the interface of the fluid and the structure domains. For the aluminium sheet in paper A, this results in a mesh that is finer than it needs to be if one just considers the needs of the structural simulation. This is not an issue, as the simulation of the structure is still several orders of magnitude less computationally demanding than the simulation of the fluid. As the CFD-software OpenFOAM is a finite volume code, the pressure is given at the cell surface centre. This pressure is assumed to be constant over the whole element and is integrated using the CALFEM element routine to obtain the nodal load vector $\mathbf{p}(t)$ in (4.1). Instead of using a constant load over each element, a more refined interpolation method could have been used. However, the increase in accuracy is deemed to be very small. Also, this would have to be implemented as there is no such implementation presently available in CALFEM.

5 Summary of the appended papers

Paper A

Load and response prediction using numerical methods in acoustic fatigue.
Johan Nilsson, Robert-Zoltán Szász, Per-Erik Austrell, Ephraim J. Gutmark.
In preparation.

This paper investigates the numerical procedure of using CFD for load prediction and then using the predicted load as input to an FE-simulation of the response of an exposed structure. The procedure is tested on a model problem consisting of a thin aluminium sheet that is located downstream of a ramped backward-facing step. The flow past the step induces a load on the aluminium sheet. Transient LES simulations are carried out to simulate the load. To keep the computational cost reasonable, the `nuSgsUSpaldingWallFunction` is used. The computed load is then used as an input to a response simulation of the aluminium sheet. The paper extends previous studies in mainly three ways. First, it attempts to use the simulated load to provide a response prediction which is not done in previous studies. The load intensities and spectral characteristics are well captured, except that the shedding frequency is overpredicted. The response prediction is reasonably well captured. When the response prediction is seen in the context of design guidelines and other studies where the load is measured, the response prediction can be seen as good. Second, it is a numerical study of the surface pressure fluctuations downstream of a backward-facing step at approximately one order of magnitude higher Reynolds numbers than previous studies. Third, it uses a wall-function for wall treatment. Previous studies on surface pressure fluctuations downstream of a backward-facing step either resolves the turbulent boundary layer in the LES sense or uses DES.

The author carried out all simulations, implemented the inlet precursor BC as well as wrote the paper. All other authors assisted in writing the paper as well as general supervision of the work. The experimental data used for comparison was provided by E. J. Gutmark.

Paper B

Numerical simulation of surface pressure fluctuations in transonic fence-like flows with high Reynolds number.
Johan Nilsson, Robert-Zoltán Szász, Per-Erik Austrell, Delphine Bard.
Submitted for publication.

This paper presents LES simulations on a transonic test case for acoustic fatigue. To keep the computational cost reasonable, the `muSgsUSpaldingWallFunction` is used. The test case is flow past an inclined fence at $\mathrm{Re}_h = 1.6 \cdot 10^6$ and $\mathrm{Ma} = 0.7$ which is realistic operating conditions for an aircraft. The simulations are compared to existing measurements from the ACOUFAT program [24]

as well as other literature on similar flows. The flow is found to be sensitive in several respects to the geometrical BC imposed. Three different geometrical configurations are therefore investigated. Several aspects of the flow and the pressure load are investigated. Most characteristics of the load are captured. In particular, the cross-spectral densities of the load are captured at a similar level as a semi-empirical model developed by Campos et al. [2]. The paper is the first numerical study on fence flow to study the surface pressure fluctuations. Also, it performs the study at three orders of magnitude higher Reynolds numbers than previous studies as well as at transonic Mach numbers which is not done before.

The author carried out all simulations as well as wrote the paper. All other authors assisted in writing the paper as well as general supervision of the work.

6 Concluding remarks and future work

6.1 Concluding remarks

In this dissertation, two model problems for acoustic fatigue have been investigated with large eddy simulation with a wall function. The focus of the research effort has been on the load prediction produced by the simulations. The aims of these simulations are to provide a load prediction without resorting to experimental methods and to improve the response prediction by also obtaining the spatial distribution of the load.

In paper A, the load intensity is well captured. The shedding frequency is overpredicted, but still within the variation found in the literature. Moreover, the spectral characteristics are well captured. Comparison of the spatial characteristics was not possible. Successful prediction of the surface pressure fluctuations downstream of a backward-facing step is itself not entirely new. However, this work takes the simulation to higher, more realistic Reynolds numbers which presents new computational challenges.

Perhaps more important for this dissertation is the response prediction performed in paper A. It shows that from a completely simulated load, a response prediction that is accurate enough to be useful can be made. The accuracy should be seen in the context of design guidelines and other studies such as the one by Cunningham et al. [3]. In this study the load intensity and distribution is determined from simulation rather than measured as it is the case in design guidelines and the study by Cunningham et al. [3]. While the results are not directly comparable the indication is that the objective of producing a good response prediction by only numerical methods appears to be met for this simple test case.

In paper B, the setting is in truly realistic Reynolds and Mach numbers. The load intensity levels and the spatial characteristics of the surface pressure fluctuations are well captured. In particular, the cross-spectral densities are captured with what appears to be a similar accuracy given by the "semi-empirical" model developed by Campos et al. [2]. It should be noted that the response prediction from the "semi-empirical" model is very good.

In addition to the promising results on the load prediction in relation to acoustic fatigue, paper B provides some interesting detail to fence flow in general by highlighting the sensitivity to the upstream conditions. The study is also the first to investigate the surface pressure fluctuations downstream of the fence and it is performed at Reynolds number two order of magnitude higher than previous numerical studies.

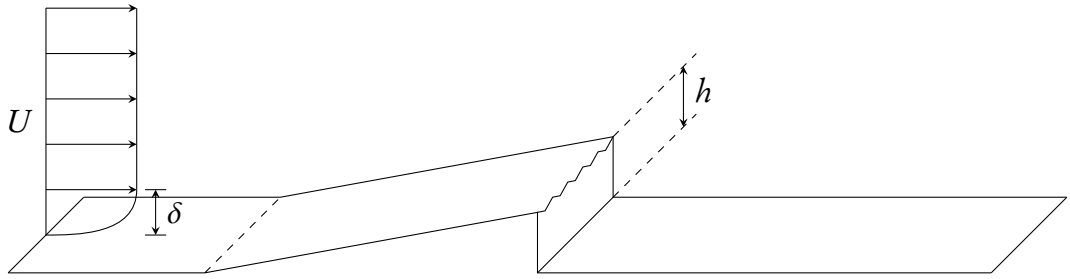

Figure 6.1: Model problem geometry with chevrons. Figure not to scale.

6.2 Proposals for future work

In this dissertation numerical methods for load prediction have been successfully developed. Perhaps most importantly, it provides a foundation to continued research. Much has been learned about their strengths and limitations. It opens possibilities to further develop the flow cases studied. One such example is the backward-facing step studied in paper A. It is suggested that if the geometry is slightly modified by adding chevrons to the step edge, then the load levels could perhaps be reduced. The setup is illustrated in Figure 6.1. The purpose of the chevrons is to destabilise the Kelvin-Helmholtz vortices that are shed from the step edge so that they break up more quickly. Chevrons are used in a similar way to reduce the noise from jet engines, see for example [67]. A stipend has also been applied for in order to investigate this setup experimentally at the University of Cincinnati under the supervision of Prof. E.J. Gutmark.

In section 3.3.3 different methods of wall treatments are discussed. In this dissertation, only results where the wall functions based on Spalding's law [48] from the equilibrium family is presented. DES was briefly tested, but did at the time not appear to give any advantage. However, the DES method was not fully explored. As it has shown great potential in many other contexts it would be interesting to explore this method further in the context of load prediction for acoustic fatigue. The study by Dietiker et al. [68] uses DES to predict the surface pressure fluctuations downstream of the backward-facing step. It appears that they predict higher load levels than what is found in the literature (this is not addressed by the authors). It would be interesting to see if this is related to the choice of DES.

In the beginning of chapter 4 the frequency domain method for the response prediction used in the ACOUFAT project [2, 24] is very briefly outlined. This method has not been tested in this dissertation as it was not readily available for the author and the main focus in the research project so far has been on load prediction. However, the method appears to be successful [2, 24] and for future work it would be interesting to combine it with load predictions from CFD simulations. The load predictions in paper B indicate that the cross-correlations needed as input to the method is captured to a similar level as the "semi-empirical" method developed by Campos et al. [2]. As the response prediction from the load given by the "semi-empirical" method was very good, this indicates a good potential for this approach worth investigating with a CFD predicted load.

References

[1] IHS ESDU (2011), *ESDU 72005, The estimation of r.m.s. stress in stiffened skin panels subjected to random acoustic loading*.

[2] Campos, L., Bourgine, A., Bonomi, B. (1999), *Comparison of theory and experiment on aeroacoustic loads and deflections*, Journal of Fluids and Structures **13**(1), 3–35.

[3] Cunningham, P., Langley, R., White, R. (2003), *Dynamic response of doubly curved honeycomb sandwich panels to random acoustic excitation. Part 2: Theoretical study*, Journal of Sound and Vibration **264**(3), 605–637.

[4] Rossiter, J. (1964), *Wind-Tunnel Experiments on the Flow over Rectangular Cavities at Subsonic and transonic Speeds*, Aeronautical Research Council Reports and Memoranda 3438.

[5] Clarkson, B. (1994), *Review of sonic fatigue technology*, NASA Technical Report CP-4587.

[6] Cunningham, P.R., White, R.G. (2004), *A review of analytical methods for aircraft structures subjected to high-intensity random acoustic loads*, Proceedings of the Institution of Mechanical Engineers, Part G: Journal of Aerospace Engineering **218**(3), 231–242.

[7] Miles, J.W. (1954), *On Structural Fatigue Under Random Loading*, Journal of the Aeronautical Sciences **21**(11), 753–762.

[8] Miner, M. (1945), *Cumulative damage in fatigue*, Journal of applied mechanics **12**(3), 159–164.

[9] Powell, A. (1958), *On the Fatigue Failure of Structures due to Vibrations Excited by Random Pressure Fields*, The Journal of the Acoustical Society of America **30**(12), 1130–1135.

[10] Clarkson, B. (1968), *Stresses in skin panels subjected to random acoustic loading*, The Aeronautical Journal of the Royal Aeronautical Society **72**, 1000–1010.

[11] Thompson, A., Lambert, R. (1972), *The estimation RMS stresses in stiffened skin panels subjected to random acoustic loading*, Technical Report Section 5, AGARD-AG-162, Advisory Group for Aerospace Research and Development.

[12] Rudder, F., Plumblee, H. (1975), *Sonic fatigue design guide for military aircraft*, Technical Report AFFDL-TR-74-112, Acoustics and Vibration Associates, Atlanta, Georgia.

[13] Blevins, R. (1989), *An approximate method for sonic fatigue analysis of plates and shells*, Journal of Sound and Vibration **129**(1), 51–71.

[14] White, R. (1978), *A comparison of some statistical properties of the responses of aluminium alloy and cfrp plates to acoustic excitation*, Composites **9**(4), 251–258.

[15] Mei, C., Prasad, C. (1987), *Effects of non-linear damping on random response of beams to acoustic loading*, Journal of Sound and Vibration **117**(1), 173–186.

[16] Reinhall, P., Miles, R. (1989), *Effect of damping and stiffness on the random vibration of nonlinear periodic plates*, Journal of Sound and Vibration **132**(1), 33–42.

[17] Green, P., Killey, A. (1997), *Time Domain Dynamic Finite Element Modelling in Acoustic Fatigue Design*, in: Ferguson, N.S., Wolfe, H.F., Mei, C. (eds.), *Proceedings of the Sixth International Conference on Recent Advances in Structural Dynamics*, 1007–1025, University of Southampton.

[18] Hollkamp, J.J., Gordon, R.W., Spottswood, S.M. (2005), *Nonlinear modal models for sonic fatigue response prediction: a comparison of methods*, Journal of Sound and Vibration **284**(3-5), 1145–1163.

[19] Blevins, R., Holehouse, I., Wentz, K. (1993), *Thermoacoustic loads and fatigue of hypersonic vehicle skin panels*, Journal of Sound and Vibration **30**(6), 971–978.

[20] Miller, B., McNamara, J., Spottswood, S., Culler, A. (2011), *The impact of flow induced loads on snap-through behavior of acoustically excited, thermally buckled panels*, Journal of Sound and Vibration **330**(23), 5736–5752.

[21] Mignolet, M.P., Przekop, A., Rizzi, S.A., Spottswood, S.M. (2013), *A review of indirect/non-intrusive reduced order modeling of nonlinear geometric structures*, Journal of Sound and Vibration **332**(10), 2437–2460.

[22] Cunningham, P., White, R. (2003), *Dynamic response of doubly curved honeycomb sandwich panels to random acoustic excitation. Part 1: Experimental study*, Journal of Sound and Vibration **264**(3), 579–603.

[23] Tougard, D. (1993), *ACOUFAT: Final technical report*, Document AERO 0025-1079 / Rept 6 / 1, ACOUFAT Project.

[24] Tougard, D. (1995), *Acoustic Fatigue and Related Damage Tolerance of Advanced Composite and Metallic Structures (ACOUFAT)*, in: Hernandez, J. M. M. (ed.), *Advances in Acoustics Technology*, 83–195, Wiley, Chichester.

[25] Campos, L. (1991), *On the correlation of acoustic pressures induced by a turbulent wake on a nearby wall*, ACOUFAT Project.

[26] Bourgine, A. (1992), *Wall pressure fluctuations and induced vibrations on a plane panel downstream a flap in transonic mach number range*, Document AERO 0025-1079 / D16 / 1, ACOUFAT Project.

[27] Onera (1991), *Definition of transonic wind tunnel test*, Document AERO 0025-1079 / D6 / 1, ACOUFAT Project.

[28] Bayerdörfer, G. (1992), *Wind tunnel- and progressive wave tube tests to determine loading actions and structural response of a stiffened al-panel*, Document AERO 0025-1079 / D12 / 1, ACOUFAT Project.

[29] *Comparison between calculated and tested results for the aluminium panel inside the wind tunnel and the progressive wave tube*, Document AERO 0025-1079 / D17 / 1, ACOUFAT Project.

[30] Wagner, C., Hüttl, T., Sagaut, P. (2007), *Large-Eddy Simulation for Acoustics*, Cambridge University Press, New York.

[31] Reynolds, O. (1883), *An Experimental Investigation of the Circumstances Which Determine Whether the Motion of Water Shall Be Direct or Sinuous, and of the Law of Resistance in Parallel Channels*, Philosophical Transactions of the Royal Society of London **174**, 935–982.

[32] Richardson, L. (1922), *Weather Prediction by Numerical Process*, Cambridge University Press.

[33] Kolmogorov, A. (1941), *The Local Structure of Turbulence in Incompressible Viscous Fluid for Very Large Reynolds Numbers*, Doklady Akademii Nauk SSSR **30**, 299–303, in Russian.

[34] Kolmogorov, A. (1991), *The Local Structure of Turbulence in Incompressible Viscous Fluid for Very Large Reynolds Numbers*, Proceedings of the Royal Society of London. Series A: Mathematical and Physical Sciences **434**(1890), 9–13.

[35] Pope, S. (2000), *Turbulent Flows*, Cambridge University Press.

[36] White, F.M. (2008), *Fluid Mechanics*, McGraw-Hill, 6th edn.

[37] Dandois, J., Garnier, E., Sagaut, P. (2007), *Numerical simulation of active separation control by a synthetic jet*, Journal of Fluid Mechanics **574**, 25–58.

[38] Ji, M., Wang, M. (2012), *Surface pressure fluctuations on steps immersed in turbulent boundary layers*, Journal of Fluid Mechanics **712**, 471–504.

[39] Hasan, M.A.Z. (1992), *The flow over a backward-facing step under controlled perturbation: laminar separation*, Journal of Fluid Mechanics **238**, 73–96.

[40] Cherry, N.J., Hillier, R., Latour, M.E.M.P. (1984), *Unsteady measurements in a separated and reattaching flow*, Journal of Fluid Mechanics **144**, 13–46.

[41] Hudy, L.M., Naguib, A.M., Humphreys, W.M. (2003), *Wall-pressure-array measurements beneath a separating/reattaching flow region*, Physics of Fluids **15**(3), 706–717.

[42] OpenFOAM Foundation (2012), *OpenFOAM, The Open Source CFD Toolbox User Guide, version 2.1.1*.

[43] Smagorinsky, J. (1963), *General circulation experiments with the primitive equations: I. The basic experiment*, Monthly Weather Review **91**(3), 99–164.

[44] Fureby, C., Tabor, G., Weller, H.G., Gosman, A.D. (1997), *A comparative study of subgrid scale models in homogeneous isotropic turbulence*, Physics of Fluids **9**(5), 1416–1429.

[45] Piomelli, U., Balaras, E. (2002), *Wall-Layer Models for Large-Eddy Simulations*, Annual Review of Fluid Mechanics **34**(1), 349–374.

[46] Cabot, W., Moin, P. (2000), *Approximate Wall Boundary Conditions in the Large-Eddy Simulation of High Reynolds Number Flow*, Flow, Turbulence and Combustion **63**(1-4), 269–291.

[47] de Villiers, E. (2006), *The Potential of Large Eddy Simulation for the Modeling of Wall Bounded Flows*, Ph.D. thesis, Imperial College of Science, Technology and Medicine, London.

[48] Spalding, D. (1961), *A Single Formula for the "Law of the Wall"*, Journal of Applied Mechanics **28**(3), 455–458.

[49] Spalart, P., Jou., W.H., Strelets, M., Allmaras, S. (1997), *Comments on the feasibility of LES for wings, and on a hybrid RANS/LES approach*, in: Liu, C., Liu, Z. (eds.), *Proceedings of the First AFOSR International Conference on DNS/LES*, 137–147, Greyden Press, Columbus.

[50] Spalart, P., Allmaras, S. (1992), *A one-equation turbulence model for aerodynamic flows*, in: *30th Aerospace Sciences Meeting and Exhibit, Reno, Nevada*, AIAA-1992-439.

[51] Spalart, P., Deck, S., Shur, M., Squires, K., Strelets, M., Travin, A. (2006), *A New Version of Detached-eddy Simulation, Resistant to Ambiguous Grid Densities*, Theoretical and Computational Fluid Dynamics **20**(3), 181–195.

[52] Spalart, P.R. (2009), *Detached-Eddy Simulation*, Annual Review of Fluid Mechanics **41**(1), 181–202.

[53] Jasak, H. (1996), *Error analysis and estimation in the finite volume method with applications to fluid flows*, Ph.D. thesis, University of London, Imperial College.

[54] Jasak, H., Weller, H., Gosman, A. (1999), *High resolution NVD differencing scheme for arbitrarily unstructured meshes*, International Journal for Numerical Methods in Fluids **31**(2), 431–449.

[55] Issa, R. (1986), *Solution of the implicitly discretised fluid flow equations by operator-splitting*, Journal of Computational Physics **62**(1), 40–65.

[56] Murugappan, S., Mihaescu, M., Dimicco, R., Gutmark, E., Landmann, A., Treiber, D., Anderson, B. (2007), *Flow-field and Acoustic Interaction behind a Ramped Step*, in: *45th AIAA Aerospace Sciences Meetings and Exhibit, Reno, Nevada*, AIAA-2007-1325.

[57] Aider, J.L., Danet, A., Lesieur, M. (2007), *Large-eddy simulation applied to study the influence of upstream conditions on the time-dependant and averaged characteristics of a backward-facing step flow*, Journal of Turbulence **8**(N51).

[58] Lund, T.S., Wu, X., Squires, K.D. (1998), *Generation of Turbulent Inflow Data for Spatially-Developing Boundary Layer Simulations*, Journal of Computational Physics **140**(2), 233–258.

[59] Timoshenko, S., Woinowsky-Krieger, S. (1959), *Theory of plates and shells*, McGraw-Hill, New York, 2nd edn.

[60] Pilkey, W. (1994), *Formulas for Stress, Strain, and Structural Matrices*, John Wiley & Sons, Inc.

[61] Austrell, P.E., Dahlblom, O., Lindemann, J., Olsson, A., Olsson, K.G., Persson, K., Petersson, H., Ristinmaa, M., Sandberg, G., Wernberg, P.A. (2004), *CALFEM - A Finite Element Toolbox version 3.4*, Studentlitteratur.

[62] Ottosen, N., Petersson, H. (1992), *Introduction to the Finite Element Method*, Prentice Hall International.

[63] Bathe, K.J. (2006), *Finite Element Procedures*, Klaus-Jürgen Bathe, Cambridge, MA.

[64] Newmark, N.M. (1959), *A Method of Computation for Structural Dynamics*, Journal of the Engineering Mechanics Division **85**(3), 67–94.

[65] Chopra, A. (2007), *Dynamics of structures: Theory and applications to earthquake engineering*, Prentice Hall, Upper Saddle River, NJ, 3rd edn.

[66] Murugappan, S., Mihaescu, M., Dimicco, R., Gutmark, E., Landmann, A., Treiber, D., Anderson, B. (2007), *Flow-field and Acoustic Interaction behind a Ramped Step*, in: *45th AIAA Aerospace Sciences Meetings and Exhibit, Reno, Nevada*, AIAA-2007-1325.

[67] Mihaescu, M., Harris, C., Dimicco, R., Gutmark, E., Fuchs, L. (2007), *Flow and Acoustics Characteristics of Chevron Nozzles in Coaxial Jets - LES & Acoustic Analogy Investigation*, in: *13th AIAA/CEAS Aeroacoustics Conference*, AIAA-2007-3609.

[68] Dietiker, J.F., Hoffmann, K.A. (2009), *Predicting Wall Pressure Fluctuation over a Backward-Facing Step Using Detached Eddy Simulation*, Journal of Aircraft **46**(6), 2115–2120.

Part II

Appended publications

Paper A

Load and response prediction using numerical methods in acoustic fatigue

Johan Nilsson[1], Robert-Zoltán Szász[2], Per-Erik Austrell[1], Ephraim J. Gutmark[3]

[1] Division of Structural Mechanics, Lund University, PO Box 118, SE-221 00, Lund, Sweden.
[2] Division of Fluid Mechanics, Lund University, PO Box 118, SE-221 00, Lund, Sweden.
[3] Department of Aerospace Engineering and Engineering Mechanics, University of Cincinnati, PO Box 210070, Cincinnati, OH 45221-0070, USA.

Abstract

A numerical procedure for load and response prediction in the context of acoustic fatigue is investigated on a model problem. Contrary to design guidelines, where the load need to be specified (e.g. based on experiments), the procedure used herein consists of simulating the load with computational fluid dynamics and then using the simulated load as a load input to a finite element simulation of the exposed structure. The model problem studied is a ramped backward-facing step with a thin aluminum panel fitted downstream of the step, parallel to the flow. The vortices generated in the wake of the step impose a time varying load on the aluminum panel. The numerical results on the load and response are compared to experimental results. The load is simulated with large-eddy simulations with a wall function. The mean reattachment length, root-mean-square pressure levels and 1/3rd octave spectrum of the pressure load on the panel compare well with the measurements while the cut-off frequency is somewhat overpredicted. The panel response prediction compares reasonably well with the measurements indicating that there is good potential for the proposed procedure to be used for load and response prediction in the context of acoustic fatigue analysis.

In preparation

Paper B

Numerical simulation of surface pressure fluctuations in transonic fence-like flows with high Reynolds number

Johan Nilsson[1], Robert-Zoltán Szász[2], Per-Erik Austrell[1], Delphine Bard[3]

[1] Division of Structural Mechanics, Lund University, PO Box 118, SE-221 00, Lund, Sweden.
[2] Division of Fluid Mechanics, Lund University, PO Box 118, SE-221 00, Lund, Sweden.
[3] Division of Engineering Acoustics, Lund University, PO Box 118, SE-221 00, Lund, Sweden.

Abstract

Surface pressure fluctuations downstream of an inclined fence are investigated with compressible, large-eddy simulations with wall-treatment. The simulations are performed at $\mathrm{Re}_h = 1.6 \cdot 10^6$ and transonic Mach numbers, which are realistic operating conditions in the aircraft industry. Simulation results are compared with existing measurements. Three different configurations are simulated to investigate the sensitivity to geometrical effects. Simulated cross-correlation spectra agreement with measurements appears to be on the level required for a good response prediction of an aircraft skin surface panel placed downstream of the fence. The mean reattachment length x_r is found to vary up to 25 % between configurations. Root-mean-square pressure fluctuation levels are found to be closer to backward-facing step flow than standard fence flow. The effect of a leading edge upstream of the fence is shown to influence the spectral characteristics of the pressure load downstream of the fence. Correlation lengths and the propagation of pressure disturbances are investigated with auto and cross-correlation maps, phase angle analysis of the cross spectrum and frequency-wavenumber spectra.

Submitted for publication